Journal of Ophthalmology

Clinical Applications of High Resolution In-Vivo Retinal Imaging

Guest Editors: Stacey S. Choi, Ann E. Elsner, Robert J. Zawadzki, and Brian Vohnsen

Clinical Applications of High Resolution In-Vivo Retinal Imaging

Journal of Ophthalmology

Clinical Applications of High Resolution In-Vivo Retinal Imaging

Guest Editors: Stacey S. Choi, Ann E. Elsner, Robert J. Zawadzki, and Brian Vohnsen

Editorial Board

Contents

Hindawi Publishing Corporation
Journal of Ophthalmology
Volume 2013, Article ID 312974, 2 pages
http://dx.doi.org/10.1155/2013/312974

Editorial

Clinical Applications of High Resolution In-Vivo Retinal Imaging

Stacey S. Choi,[1] Ann E. Elsner,[2] Robert J. Zawadzki,[3] and Brian Vohnsen[4]

[1] *Department of Vision Science, New England College of Optometry, Boston, MA 02115, USA*
[2] *School of Optometry, Indiana University, Bloomington, IN 47405-3680, USA*
[3] *Department of Ophthalmology and Vision Science, University of California, Davis, Sacramento, CA 95817, USA*
[4] *School of Physics, University College Dublin, Dublin 4, Ireland*

Correspondence should be addressed to Stacey S. Choi; chois@neco.edu

Received 31 January 2013; Accepted 31 January 2013

The last two decades have witnessed major advancements in retinal imaging technologies thanks, in no small part, to improved light sources and detectors, adaptive optics, and high-speed computers. New research grade systems are continuously improving [1] and some have obtained a degree of user friendliness and robustness that have facilitated their transition to clinical use. Ultrahigh resolution commercial scanning laser ophthalmoscopy (SLO) and optical coherence tomography (OCT) systems are becoming commonplace in modern ophthalmic clinics where they provide often unprecedented image quality with resolving powers down to the level of single retinal cells in the living eye. Such richness in detail provides challenges and possible paradigm shifts, but already an enormous impact on improved diagnostics has been realized as we continue to work towards the ultimate goal of achieving healthy vision throughout life.

The six papers included in this special issue cover some of the recent advances on the clinical applications of high resolution, in vivo retinal imaging using an array of leading imaging technologies and in particular spectral-domain- (SD-) OCT. While SD-OCT has been widely accepted for retinal imaging little more than a decade ago, it has rapidly become the method of choice for fast ultrahigh resolution cross-sectional imaging that produces histology-like results, as well as 3D imaging of structures within the eye [2]. With broadband spectral illumination, axial resolution on the order of 2-3 microns [3] has become possible, which is close to the transverse resolution limit of about 2 microns achievable with adaptive optics and dilated pupil [4].

One of the chief concerns in the ageing population is age-related macular degeneration (AMD), as it can have a detrimental impact on the life quality of affected individuals. A number of risk factors for AMD development have been identified. The majority of cases present as dry AMD, in which the appearance of deposits hidden beneath the retina, called drusen, provides an early sign of the disease. The less common wet AMD is typically more severe, with development of new vessels that leak and lead to the formation of scars. It is the wet AMD that leads more often to a rapid and debilitating loss of central vision. B. Wolff et al. show imaging results of outer retinal tubulations that can form as a consequence of wet AMD. *En face*, ultrahigh resolution SD-OCT scans in the transverse direction show a network of scarring in what the authors term as "pseudodendritic."

The neurodegenerative Parkinson's disease (PD) is another concern in the ageing population that relates to protein aggregation of amyloid fibers in the brain but also has implications for the eye and vision. E. M. Shrier et al. report on SD-OCT scans of foveal thickness in PD patients in relation to a thinning of the nerve fiber layer. To differentiate between retinal layers, they focused their study on the foveal pit and found that about half of the patients had substantial intraocular asymmetry of the slope of the foveal pit slightly off-axis from the foveola. Thus, these differences may potentially be used as indicators of PD.

The review article by Y. Barak et al. discusses the ageing process of the vitreoretinal interface, vitreous shrinkage, and associated pathologies visualized with SD-OCT. Examples described include posterior vitreous detachment and the development of floaters, vitreomacular traction causing retinal swelling and reduced vision, and macular holes that may develop into full thickness macular holes requiring surgical intervention to prevent vision loss. The paper also discusses future perspectives including the exciting possibility of intraoperative SD-OCT that will allow real-time monitoring of changes taking place during macular surgery.

Two commercial SD-OCT and time-domain OCT instruments are compared in a study of retinal nerve fiber layer thickness in 132 healthy subjects by I. Pinilla et al. Both techniques give similar results of 95 to 98 micron thickness, though the accuracy is found to be higher with SD-OCT in agreement with also other studies. Retinal nerve fiber layer thickness is related to early diagnosis of glaucoma, in which accurate determination of thinning is of utmost importance.

A comparison of SD-OCT and time-domain OCT instruments is again central in the work by A. P. Lange et al. related to retinal nerve fiber layer thickness in the eyes of multiple sclerosis (MS) patients suffering from optic neuritis. A systematic 2-micron difference in measured thickness is reported between the two instruments, similar to the conclusion reached by I. Pinilla et al. This stresses the importance of specifying the device used in any comparative study. MS patients have a thinner retinal nerve fiber layer thickness in comparison to a control group, and in particular MS patients with a history of optic neuritis show a substantial reduction in the retinal nerve fiber layer thickness.

The final paper by S. Kawaguchi et al. deals with ocular blood flow, carotid revascularization surgery, and chronic ocular ischemic syndrome. Color-coded Doppler flow imaging before and after revascularization surgery confirmed an increased flow velocity, and visual acuity increased in 60% of the patients.

All six papers in this special issue have undergone a rigorous peer review process, and we are thankful to the referees for their work to meet the quality requirements of the accepted papers to ensure that it conforms to the standards of the Journal of Ophthalmology. We hope that the readers will find the papers of interest as they show essential parts of the spectrum of clinical work already being done with ultrahigh and high resolution retinal imaging techniques and that they may inspire future clinical work. Given the relatively novelty of ultrahigh resolution retinal imaging technologies, the future looks promising for much improved diagnostic imaging as the limits of the methods are removed and their clinical usage continues to grow.

Stacey S. Choi
Ann E. Elsner
Robert J. Zawadzki
Brian Vohnsen

References

[1] J. Carroll, M. Pircher, and R. J. Zawadzki, "Introduction: feature issue on cellular imaging of the retina," *Biomedical Optics Express*, vol. 2, no. 6, pp. 1778–1780, 2011.

[2] M. Wojtkowski, R. Leitgeb, A. Kowalczyk, T. Bajraszewski, and A. F. Fercher, "In vivo human retinal imaging by Fourier domain optical coherence tomography," *Journal of Biomedical Optics*, vol. 7, no. 3, pp. 457–463, 2002.

[3] W. Drexler and J. G. Fujimoto, "State-of-the-art retinal optical coherence tomography," *Progress in Retinal and Eye Research*, vol. 27, no. 1, pp. 45–88, 2008.

[4] P. Godara, A. M. Dubis, A. Roorda, J. L. Duncan, and J. Carroll, "Adaptive optics retinal imaging: emerging clinical applications," *Optometry and Vision Science*, vol. 87, no. 12, pp. 930–941, 2010.

Hindawi Publishing Corporation
Journal of Ophthalmology
Volume 2012, Article ID 350475, 6 pages
doi:10.1155/2012/350475

Clinical Study

Ocular Circulation and Chronic Ocular Ischemic Syndrome before and after Carotid Artery Revascularization Surgery

Shoichiro Kawaguchi, Jun-ichi Iida, and Yoshitomo Uchiyama

Department of Neurosurgery, Nara Prefectural Nara Hospital, Nara 631-0846, Japan

Correspondence should be addressed to Shoichiro Kawaguchi, skawaguc@naramed-u.ac.jp

Received 5 March 2012; Revised 14 October 2012; Accepted 15 November 2012

Academic Editor: Stacey S. Choi

Background. We evaluated the effect of carotid revascularization surgery on ocular circulation and chronic ocular ischemic syndrome (OIS). *Methods*. We examined ninety patients with carotid artery stenosis (more than 50% stenosis) at its origin treated with carotid endarterectomy ($N = 56$) or carotid artery stenting ($N = 34$). Twenty-five patients (28%) complained of chronic OIS. Ocular circulation was examined before and after revascularization surgery using ophthalmic artery (OphAr) and central retinal artery (CRA) color Doppler flow imaging. *Results*. (1) Ocular circulation: preoperatively, the average OphAr peak systolic flow velocity (Vs) was 0.05 m/sec, and the average CRA Vs was 0.07 m/sec. At 1 week after surgery, the average OphAr Vs significantly increased to 0.32 ($P < 0.05$), and the average CRA Vs significantly increased to 0.11 m/sec ($P < 0.05$). These significant improvements were sustained throughout the three months of the followup. (2) OIS: during the follow-up period (mean: 3.6 years), 15 patients (60%) showed visual acuity improvement, and no patients complained of amaurosis fugax or worsening of the chronic OIS. *Conclusion*. Carotid revascularization surgery was effective in improving the ocular circulation, and it was also useful for the chronic OIS due to the carotid artery stenosis.

1. Introduction

One of the important clinical aspects of internal carotid artery stenosis at its origin is the influence on the flow dynamics of the ocular circulation. The blood supply to the eye is mostly provided by branches of the ophthalmic artery (OphAr), which is a branch of the internal carotid artery. This is why many patients with cerebral ischemia in the internal carotid artery may present with ipsilateral visual symptoms [1]. The disturbed ocular circulation correlates with chronic ocular ischemic syndrome symptoms such as frequent amaurosis fugax or a decline of visual acuity [2, 3]. Carotid revascularization surgery, such as carotid endarterectomy (CEA) and carotid artery stenting (CAS), may also restore the cerebral perfusion pressure and improve the intracranial vascular hemodynamics including ocular circulation. Therefore, carotid artery revascularization surgery reduces the risk of stroke in symptomatic and asymptomatic patients [4, 5]. Despite this well-established benefit, there have been few reports concerning the effect of carotid revascularization surgery on ocular circulation. Therefore, it is significant to understand the ocular circulation and ocular symptoms in patients with internal carotid artery stenosis before and after CAS.

In this study, we discussed and analyzed the effect of carotid revascularization surgery on the ocular circulation and chronic ocular symptoms in patients with carotid artery stenosis.

From January 2002 through January 2012, we examined the ocular circulation in 90 consecutive patients showing internal carotid artery origin stenosis (more than 50%) treated with CEA or CAS. Eighty patients were males, and 10 were females. Their ages ranged from 47 to 81 years, with a mean of 69 years. The clinical symptoms of the patients were transient ischemic attack in 65 patients, stroke in 13, and asymptomatic in 12.

According to the criteria of the NASCET study [4], the grades of angiographical internal carotid artery stenosis on the ipsilateral side were more than 60% stenosis in 10 patients, more than 70% stenosis in 17, more than 80%

stenosis in 13, more than 90% stenosis in 34, and more than 95% stenosis in 16. Among the 90 patients, 25 complained of chronic ocular ischemic syndrome. All these 25 patients had visual acuity of 20/40 or worse, and 9 patients among them had frequent amaurosis fugax. No patients showed blindness. The exclusion criteria for chronic ocular ischemic syndrome were acute ocular ischemic symptoms such as sudden loss of vision, a single episode of amaurosis fugax, or ocular/orbital pain [6].

Carotid revascularization surgery was performed at least 4 weeks after the last attack. Within 2 weeks after the procedure, the patency of the treated carotid artery was confirmed by carotid angiography, MRA, or ultrasonography. No patients complained of a permanent neurological deficit due to the surgery.

All patients were followed up for the clinical symptoms after carotid revascularization. The follow-up period was 0.5 to 4.5 years (mean: 3.6 years). During this period, none of the patients had a recurrent ischemic attack or worsening of the symptoms including the ocular signs.

2. Methods

To evaluate the ocular circulation, we examined the OphAr flow and central retinal artery (CRA) flow using color Doppler flow imaging (CDFI) with a 5-MHz phased linear probe; the mechanical index was less than 0.23, and the examination was completed within 3 minutes in each eye.

While the patient was supine, the probe was applied to the closed eyelids. During the examination, minimal pressure was applied to the globe to avoid the damage to the globe and artifacts. With the probe resting on the closed eyelids, the ultrasound beam was directed posteriorly in the orbit. After systematic scanning of the orbit, the OphAr and CRA were imaged, and spectral velocity analysis was performed. Pulsed Doppler spectrum analyses were recorded from the OphAr and CRA [7]. Blood flow was monitored continuously, and we employed a Doppler angle of 60° or less for each measurement [8]. Each Doppler waveform was automatically drawn and calculated using the software included with the ultrasound system. The OphAr was examined approximately 20 mm behind the globe as the vessel parallel to the nasal border of the optic nerve just after crossing it, and the CRA was examined within 5 mm of the retrolaminar portion of the optic nerve (Figure 1) [8]. The OphAr and CRA CDFI findings from the ipsilateral side of revascularization surgery were analyzed. The OphAr and CRA CDFI were performed within 1 week before surgery and at 1 week, 1 month, and 3 months after surgery in each patient. These CDFI studies provided information regarding the flow direction and peak systolic flow velocity of the OphAr and CRA.

We also performed OphAr and CRA CDFI on 51 normal healthy volunteers. Their mean age was 68 years; 28 volunteers were males, and 23 were females. The average peak systolic flow velocities were 0.35 ± 0.13 m/sec in the OphAr and 0.12 ± 0.04 m/sec in the CRA. All volunteers showed normal OphAr flow direction, that is, flow away from the orbital apex to the globe.

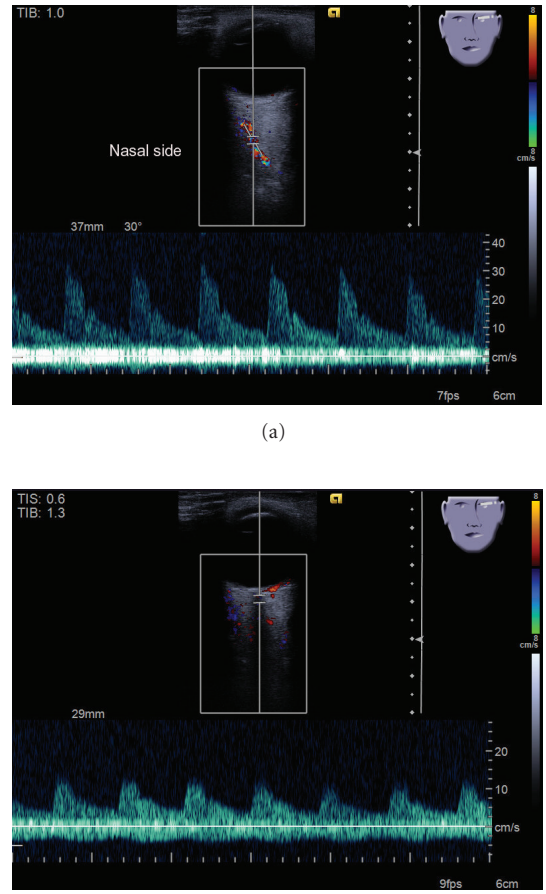

Figure 1: Color Doppler flow imaging of the ophthalmic artery (a) and central retinal artery (b) in normal control.

All patients were examined in terms of their ocular symptoms such as visual acuity and amaurosis fugax before the CEA or CAS procedure and during the follow-up period.

The physiological data were compared using two-tailed paired Student's t-test and chi-square test. A value of $P < 0.05$ was considered as the threshold for statistical significance. All values are reported as mean ± standard deviation (SD).

3. Results

3.1. Ocular Circulation (Table 1)

3.1.1. Before Surgery. The OphAr flow directions were reversed in 25 patients and antegrade in 65 patients. The average OphAr peak systolic flow velocity was 0.05 ± 0.34 m/sec, and the average CRA peak systolic flow velocity was 0.08 ± 0.02 m/sec. These values were significantly low compared with those of the controls ($P < 0.05$).

There was a statistically significant difference ($P < 0.05$) between the values of the average CRA peak systolic flow velocity in the patients with reversed OphAr flow, which was 0.06 ± 0.01 m/sec, and antegrade OphAr flow, which was 0.08 ± 0.02 m/sec.

Table 1: Course of peak systolic flow velocity (m/sec).

	Ophthalmic artery	Central retinal artery
Before surgery	0.05 ± 0.34	0.08 ± 0.02
At 1 week after surgery	0.32 ± 0.12	0.11 ± 0.03
At 1 month after surgery	0.31 ± 0.13	0.11 ± 0.04
At 3 months after surgery	0.32 ± 0.12	0.12 ± 0.04

$^*P < 0.05$.

3.1.2. After Surgery. At 1 week after surgery, the patients showing reversed OphAr flow before surgery all returned to the normal antegrade OphAr flow. This correction of the reversed OphAr flow was significant ($P < 0.05$). At 1 month and 3 months after surgery, the significant correction of the ophthalmic artery flow was sustained. At one week after surgery, the average OphAr peak systolic flow velocity significantly increased to 0.32 ± 0.12 m/sec ($P < 0.05$), and the average CRA peak systolic flow velocity also significantly increased to 0.11 ± 0.03 m/sec ($P < 0.05$). These significant increases of the average OphAr and CRA peak systolic flow velocities were sustained throughout the three months of the followup.

3.2. Ocular Symptoms. Before surgery, 25 patients complained of chronic ocular ischemic syndrome. Among these 25 patients, 15 showed reversed OphAr flow direction, and the other 10 patients showed antegrade flow. The relationship between the presence of chronic ocular ischemic syndrome and reversed OphAr flow direction was significant ($P < 0.05$). In addition, the average OphAr and CRA peak systolic flow velocities were significantly low ($P < 0.05$) in the patients with chronic ocular ischemic syndrome compared with those in the patients without chronic ocular ischemic syndrome (Table 2). Among 25 patients with chronic ocular ischemic syndrome before surgery, 15 patients (60%) showed improvement of visual acuity during the follow-up period, but 10 patients had no improvement of visual acuity, even with normal ophthalmic flow after surgery. This failure might have been due to irreversible neovascular glaucoma. In each patient, amaurosis fugax was not seen during the follow-up period.

4. Patients

Sixty-five patients showed no chronic ocular ischemic syndrome before surgery. During the follow-up period, these 65 patients complained of no chronic ocular ischemic syndrome, such as disturbance of visual acuity and frequent amaurosis fugax.

4.1. Illustrative Case. A 77-year-old man was referred to our hospital complaining of transient right hemiparesis and left visual acuity decline. Left carotid angiography showed 98% stenosis of the right internal carotid artery at its origin (Figure 2(a)). The left OphAr CDFI showed reversed flow, and the peak systolic flow velocity was −0.62 m/sec (Figure 2(b)). The left CRA peak systolic flow velocity

Table 2: Relationship between chronic ocular ischemic syndrome and ocular circulation.

	Chronic ocular ischemic syndrome		
	Positive		Negative
Peak systolic flow velocity (m/sec)			
Ophthalmic artery	−0.19 ± 0.4	($P < 0.05$)	0.14 ± 0.26
Central retinal artery	0.06 ± 0.01	($P < 0.05$)	0.08 ± 0.02
Ophthalmic artery flow direction (cases)			
Antegrade	10	($P < 0.05$)	55
Reversed	15		10

was 0.06 m/sec (Figure 2(c)). Left CEA was performed. Postoperative carotid angiography showed the good patency of the carotid artery (Figure 2(d)). At 1 week after CEA, the left OphAr CDFI showed resolution of the reversed flow, and the peak flow velocity was 0.30 m/sec (Figure 2(e)). The peak systolic flow velocity of the CRA was 0.12 m/sec (Figure 2(f)). At 1 month and 3 months after CEA, there was no marked change of the peak systolic flow velocity of OphAr and CRA.

The right visual acuity gradually improved at 3 months after CEA. The patient was followed up for 2.8 years after CEA, and there were no neurological ischemic events including visual symptoms.

5. Discussion

Patients with internal carotid artery occlusion or stenosis develop ocular ischemia because these diseases reveal the hemodynamic reduction of ocular circulation [9]. The presentation of ocular signs can vary considerably may be quite varied, with some cases showing rapid advancement of neovascularization following high intraocular pressure [10, 11]. Neovascular glaucoma secondary to internal carotid artery occlusion is usually resistant to treatment [11]. Moreover, carotid artery occlusion often progresses without symptoms, and when the patient notices an ocular disorder and visits a clinic, the condition is often at an advanced stage of ocular ischemia, in which neovascular glaucoma has developed with severe internal carotid artery stenosis [11]. Therefore, it is significant to evaluate the ocular circulation to detect and prevent ocular ischemia in patients with internal carotid artery stenosis treated with a CEA or CAS procedure. We previously reported the effect of

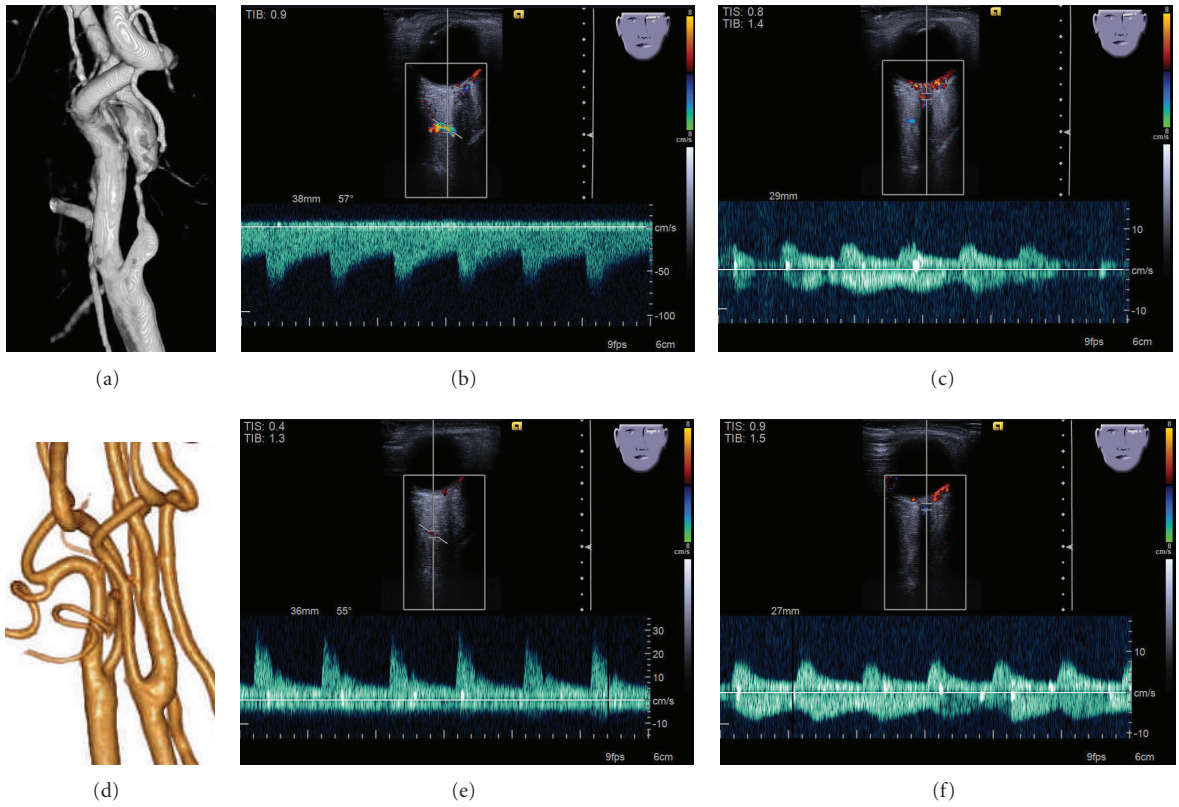

Figure 2: Left carotid angiography (a), ophthalmic artery Doppler flow imaging (b), and central retinal artery Doppler flow imaging (c) before carotid endarterectomy were shown. 3D CT angiography (d), ophthalmic artery Doppler flow imaging (e), and central retinal artery Doppler flow imaging (f) after carotid endarterectomy were shown.

superficial temporal artery to middle cerebral artery (STA-MCA) bypass, CEA, and CAS on the OphAr flow [12–14]. However, there have been few reports about the effect of carotid revascularization surgery on the ocular circulation and ocular ischemic syndrome. In this study, we evaluated the effect of carotid revascularization surgery, such as CEA and CAS, on chronic ocular ischemic syndrome and ocular circulation, including the OphAr flow and CRA flow, before and after surgery as well as during the follow-up period.

Reversed OphAr flow seen in the patients with carotid artery stenosis may contribute to the development of ocular ischemic syndrome [2]. In these patients, the ophthalmic artery might function as collateral circulation from the extracranial to the intracranial circulation [15]. When severe internal carotid artery stenosis occurs in patients with incomplete blood circulation in the circle of Willis, the blood flow in the OphAr reverses to supply the ipsilateral brain. This so-called "steal phenomenon" results in ocular ischemia, the prolongation of which leads to rubeosis iridis and neovascular glaucoma [9]. In this series, 25 patients showed reversed OphAr flow before CEA or CAS, and the reversed ophthalmic artery flow was significantly seen in the 15 patients (60%) showing chronic ocular ischemic syndrome before revascularization surgery in this series.

Yamamoto et al. established four eye types based on the retrobulbar blood flow direction [9]: forward OA, CRA, and short posterior ciliary artery (SPCA) flow (type 1); reverse OA and forward CRA and SPCA flow (type 2a); reverse OA and undetectable CRA and SPCA flow (type 2b); and undetectable flow in all three arteries (type 3). In type 2b eyes, almost the entire collateral circulation via the OphAr was deviated towards the internal carotid artery, reducing the blood flow to the eye. Rubeosis iridis occurred in half of them. In type 3, no collateral blood supply developed. Therefore, the ocular end circulation was markedly reduced, possibly because of insufficient collateral circulation via both the circle of Willis and the external carotid artery system. Rubeosis iridis was seen in one-third. In our series, 15 patients with reversed OphAr flow showed ocular ischemic syndrome, and those patients also showed the significantly reduced CRA flow. Therefore, eyes with reversed OphAr flow and low CRA peak systolic flow velocity may be at greater risk for ocular ischemic syndrome.

Carotid artery revascularization reduces the risk of stroke in symptomatic and asymptomatic patients [5]. Improvements in surgical and endovascular techniques have reduced the incidence of ischemic stroke following CEA and CAS, respectively. In this series, after the carotid revascularization surgery, the average OphAr and CRA peak systolic flow velocities improved to the normal control levels. Moreover, after the carotid revascularization surgery, the flow direction of the OphAr became normal in all cases showing reversed

OphAr flow before surgery. This significant improvement in the ophthalmic artery flow velocity also explains the correction of ocular hemodynamic compromise.

In this study, improvement in the peak systolic flow velocity of the OphAr and CRA flows and the normalization of the reversed OphAr flow occurred 1 week after revascularization surgery. The significant improvements of the average OphAr and CRA peak systolic flow velocities and the correction of the ophthalmic artery flow direction were sustained throughout the three months of followup. These effects of carotid revascularization surgery were highly expected. We clarified the chronological improvement of the disturbed OphAr and CRA peak systolic flow velocities and the correction of the reversed OphAr flow direction after revascularization surgery using the OphAr and CRA CDFI findings. The OphAr and CRA CDFI findings provide clear evidence of hemodynamic compromise in carotid artery stenosis. We proved the significantly increased flow velocity and corrected flow direction of the ocular circulation in all patients immediately after CEA and CAS.

For the patients with chronic ocular ischemic syndrome due to disturbed ocular circulation, it is vital to correct the ocular circulation to prevent and improve ocular ischemia [15]. In this series, 25 patients showed chronic ocular ischemic syndrome. Among them, 15 patients showed reversed ophthalmic artery flow initially. After CEA or CAS, the reversed ophthalmic artery flow in all of these 15 patients was resolved. Therefore, revascularization surgery is the appropriate treatment maneuver for patients with ocular ischemic syndrome due to reversed ophthalmic artery flow revealed from severe internal carotid artery stenosis. The other 10 patients among those with chronic ocular ischemic syndrome showed antegrade ophthalmic artery flow with reduction of peak systolic flow velocity before CAS or CEA. In these patients, OphAr and CRA peak systolic flow velocities significantly increased immediately after CAS procedure. Fifteen patients showed improvement of the visual symptoms after surgery. Ten patients showed no improvement of the chronic ocular ischemic syndrome due to irreversible optic apparatus lesion.

We report clear evidence of the effect of CEA and CAS on the improvement and prevention of chronic ocular ischemia due to internal carotid artery stenosis, on the basis of data obtained from OphAr and CRA CDFIs and clinical symptoms. Therefore, there is a good correlation between the course of ocular ischemic syndrome and the improvement of the ophthalmic artery CDFI findings during the follow-up period. CEA and CAS are effective for the treatment and prevention of ocular ischemic syndrome and are most beneficial if performed early, before the onset of irreversible neovascular glaucoma or irreversible ischemic optic fundi [10].

Since Lieb et al. [16] first reported CDFI as a reliable means of evaluating ocular circulation, and it has been used to measure retrobulbar blood flow in occlusive carotid artery disease patients and to confirm the presence of the steal phenomenon [9]. CDFI of the ocular circulation is a noninvasive, repeatable technique for measuring orbital blood flow. The hemodynamic parameters of CDFI are not sex dependent and do not vary between orbits [9]. The OphAr is easily visualized deep in the orbital cavity, in the area where it crosses the optic nerve; the spectral analysis is typical, displaying a pulsatile and positive waveform with blood flow velocity of 35 ± 11 cm/sec [17]. In the present series, OphAr and CRA could also be detected using orbital color Doppler flow imaging in all patients and normal volunteers. Reliability problems can arise when blood flow monitoring is performed in small ocular arteries or in veins because the lower velocities found in these vessels are close to the resolution limit for detection using the ultrasonographic system (when the flow rate, e.g., falls below 1–3 cm/sec in central retinal vein occlusion) [17]. Ultrasonographic waves can damage the eye tissues, particularly from heat; therefore, the avoidance of prolonged imaging is recommended, as is the reduction of output energy [18]. In our series, the MI was less than 0.23, and examination time was less than 3 minutes.

6. Conclusion

In patients with carotid artery stenosis, reversed OphAr flow is related to the decrease of CRA peak systolic flow velocity and the occurrence of chronic ocular ischemic syndrome. Carotid revascularization surgery achieved normalization of the disturbed OphAr flow and CRA flow, whether the flow direction of the OphAr was reversed or antegrade, immediately after revascularization surgery. CEA and CAS improved the chronic ocular ischemic syndrome revealed from severe carotid artery stenosis and also prevented the progression and onset of chronic ocular ischemic syndrome.

References

[1] C. Lamirel, N. J. Newman, and V. Biousse, "Vascular neuro-ophthalmology," *Handbook of Clinical Neurology*, vol. 93, pp. 595–611, 2009.

[2] V. P. Costa, S. Kuzniec, L. J. Molnar, G. G. Cerri, P. Puech-Leao, and C. A. Carvalho, "Clinical findings and hemodynamic changes associated with severe occlusive carotid artery disease," *Ophthalmology*, vol. 104, no. 12, pp. 1994–2002, 1997.

[3] L. H. Y. Young and R. E. Appen, "Ischemic oculopathy. A manifestation of carotid artery disease," *Archives of Neurology*, vol. 38, no. 6, pp. 358–361, 1981.

[4] D. W. Taylor and H. J. M. Barnett, "Beneficial effect of carotid endarterectomy in symptomatic patients with high-grade carotid stenosis," *The New England Journal of Medicine*, vol. 325, no. 7, pp. 445–453, 1991.

[5] P. M. Rothwell, M. Eliasziw, S. A. Gutnikov et al., "Analysis of pooled data from the randomized controlled trials of endarterectomy for symptomatic carotid stenosis," *The Lancet*, vol. 361, pp. 107–116, 2003.

[6] J. B. Mizener, P. Podhajky, and S. S. Hayreh, "Ocular ischemic syndrome," *Ophthalmology*, vol. 104, pp. 859–864, 1997.

[7] R. C. Sergott, P. M. Flaharty, W. E. Lieb et al., "Color Doppler imaging identifies four syndromes of the retrobulbar circulation in patients with amaurosis fugax and central retinal artery occlusions," *Transactions of the American Ophthalmological Society*, vol. 90, pp. 383–402, 1992.

[8] S. Takayama, M. Watanabe, H. Kusuyama et al., "Evaluation of the effects of acupuncture on blood flow in humans with

ultrasound color Doppler imaging," *Evidence-Based Complementary and Alternative Medicine*, vol. 2012, Article ID 513638, 8 pages, 2012.

[9] T. Yamamoto, K. Mori, T. Yasuhara et al., "Ophthalmic artery blood flow in patients with internal carotid artery occlusion," *British Journal of Ophthalmology*, vol. 88, pp. 505–508, 2004.

[10] K. Riihelainen, M. Paivansalo, I. Suramo, and L. Laatikainen, "The effect of carotid endarterectomy on ocular blood velocity," *Ophthalmology*, vol. 104, no. 4, pp. 672–675, 1997.

[11] A. Kodama, K. Sugioka, K. Kuniyoshi, S. Okuyama, C. Matsumoto, and Y. Shimomura, "Intravitreal bevacizumab injection and carotid artery stent replacement for neovascular glaucoma in internal carotid artery occlusion," *Clinical Ophthalmology*, vol. 4, no. 1, pp. 1177–1180, 2010.

[12] S. Kawaguchi, T. Sakaki, T. Morimoto, S. Okuno, and N. Nishikawa, "Effects of bypass on ocular ischaemic syndrome caused by reversed flow in the ophthalmic artery," *The Lancet*, vol. 354, no. 9195, pp. 2052–2053, 1999.

[13] S. Kawaguchi, S. Okuno, T. Sakaki, and N. Nishikawa, "Effect of carotid endarterectomy on chronic ocular ischemic syndrome due to internal carotid artery stenosis," *Neurosurgery*, vol. 48, no. 2, pp. 328–333, 2001.

[14] S. Kawaguchi, T. Sakaki, H. Iwahashi et al., "Effect of carotid artery stenting on ocular circulation and chronic ocular ischemic syndrome," *Cerebrovascular Diseases*, vol. 22, no. 5-6, pp. 402–408, 2006.

[15] H. H. Hu, S. Wang, C. M. Chern et al., "Clinical significance of the ophthalmic artery in carotid artery disease," *Acta Neurologica Scandinavica*, vol. 92, pp. 242–246, 1995.

[16] W. E. Lieb, P. M. Flaharty, R. C. Sergott et al., "Color Doppler imaging provides accurate assessment of orbital blood flow in occlusive carotid artery disease," *Ophthalmology*, vol. 98, no. 4, pp. 548–552, 1991.

[17] T. H. Williamson and A. Harris A, "Color Doppler ultrasound imag¬ing of the eye and orbit," *Survey of Ophthalmology*, vol. 40, pp. 255–267, 1996.

[18] P. Cattaneo, P. Marchetti, V. D. Bruno, G. Mariscalco, and A. Sala, "Color Doppler imaging of the ophthalmic artery: during antegrade selective cerebral perfusion," *Texas Heart Institute Journal*, vol. 34, no. 1, pp. 105–107, 2007.

Hindawi Publishing Corporation
Journal of Ophthalmology
Volume 2012, Article ID 542417, 3 pages
doi:10.1155/2012/542417

Clinical Study

En Face OCT Imaging for the Diagnosis of Outer Retinal Tubulations in Age-Related Macular Degeneration

Benjamin Wolff, Alexandre Matet, Vivien Vasseur, José-Alain Sahel, and Martine Mauget-Faÿsse

Rothschild Ophthalmologic Foundation, 25 rue Manin, 75019 Paris, France

Correspondence should be addressed to Benjamin Wolff, bwolff@hotmail.fr

Received 3 March 2012; Revised 22 July 2012; Accepted 1 August 2012

Academic Editor: Robert J. Zawadzki

Purpose. "En face" is an emerging imaging technique derived from spectral domain optical coherence tomography (OCT). It produces frontal sections of retinal layers, also called "C-scan OCT." Outer retinal tubulations (ORTs) in age-related macular degeneration (AMD) are a recent finding evidenced by spectral-domain OCT. The aim of this study is to characterize the morphology of ORT according to the form of AMD, using "en-face" spectral domain OCT. *Methods*. "En face" OCT imaging was prospectively performed in 26 consecutive eyes with AMD that also had ORT. *Results*. There were 15 neovascular, 8 atrophic, and 3 eyes with a mixed (fibrotic and atrophic) form of AMD. Among the neovascular group, the most frequent tubulation pattern on "en-face" OCT was a branching network emanating from a fibrovascular scar; we term this pattern as "pseudodendritic." It did not require treatment when observed as an isolated finding. In all cases of atrophic AMD, the tubular network was located at the edge of the geographic atrophy area, and formed a "perilesional" pattern. Six atrophic cases showed tubular invaginations inside this area. *Conclusion*. "En face" OCT is a valuable technique in the diagnosis and followup of macular disease. It revealed the main characteristic patterns of ORT associated with neovascular and atrophic AMD.

1. Introduction

Outer retinal tubulations (ORT) have been recently identified in age-related macular degeneration (AMD) thanks to technological improvements in Spectral-Domain Optical Coherence Tomography (SD-OCT) [1]. ORT usually have a characteristic presentation, and thus can be easily diagnosed. It is of clinical significance to recognize them, since they do not indicate ongoing exudative process and, therefore, do not require treatment.

On B-scans ORT are round hyporeflective lesions, which may contain a few focal hyperreflective spots, and are always delineated by an hyperreflective ring, in contrast to the completely hyporeflective retinal cystoid lesions. They are always located at the level of the outer nuclear layer, and in AMD are classically found very close to areas of neovascular fibrosis or retinal atrophy. These lesions have been named "tubulations" because they exhibit a tubular morphology when observed in frontal sections using "en face" OCT scans, also called C-scans.

This study aims to differentiate between the ORT presentations observed by "en face" OCT in exudative and atrophic AMD.

2. Methods

Eyes with a diagnosis of neovascular or atrophic AMD, and demonstrating ORT on SD-OCT, were prospectively studied using "en face" OCT. For all cases, systematic work-up included macular examination by SD-OCT (Spectralis Heidelberg Engineering, Heidelberg, Germany) and macular mapping consisting of 197 transverse sections in a $5.79 \times 5.79\,\text{mm}^2$ central retinal area. Tridimensional reconstruction generated by the pooling of these sections provided a virtual macular brick, through which 496 shifting sections in the coronal plane resulted in C-scan, or "en face" OCT,

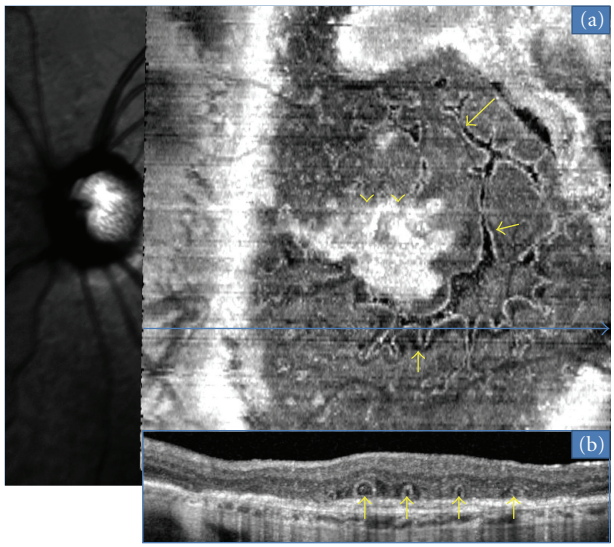

Figure 1: ORT (arrows) located above a fibrovascular scar (arrows heads). A branching network is observed emanating from hyper reflective the fibrovascular scar with numerous ramifications (or "pseudodendritic" pattern) is observed with "en face" OCT (a). Corresponding B-scan (b) demonstrates multiples ORT.

while B-scan, or conventional OCT, is derived from sagittal and transverse sections. These results were then compared with data from classical retinal imaging, namely, fundus photography and angiography. For all eyes with atrophic AMD, autofluorescence imaging was also performed.

3. Results

Twenty-six eyes of 23 AMD patients demonstrating ORT on B-scan SD-OCT were analyzed by "en face" OCT. Neovascular AMD with a neovascular fibrotic scar was identified in 15 eyes, geographic atrophy in 8 eyes and "mixed" exudative and atrophic AMD form in 3 eyes.

In the 15 neovascular fibrotic scar cases, the most frequent finding regarding ORT was a branching network emanating from a fibrovascular scar ($n = 11$) with numerous ramifications (or digitations) resulting in a "pseudodendritic" pattern (Figure 1). In all 4 remaining eyes, ORT had a tubular shape, appearing round in B-scans, with no or limited digitations (Figure 2). The fibrotic neovascular choroidal network was formally identified in all 15 eyes as a hyperreflective lesion above the level of the retinal pigment epithelium. Associated intraretinal cystoid cavities related to neovascular reactivation or the progression of retinal degeneration were observed in 7 cases (Figure 3).

In all the 8 geographic atrophy AMD cases, ORT also exhibited a round section on B-scan. However, C-scans showed that these tubulations followed the margins of the chorioretinal atrophic area (Figure 4). This ORT aspect was then termed "perilesional." Correlation with autofluorescence imaging demonstrated that ORT did not extend beyond the hyperreflective border of the atrophic area. Invaginations of ORT inside the atrophic zone were also found in 6 cases.

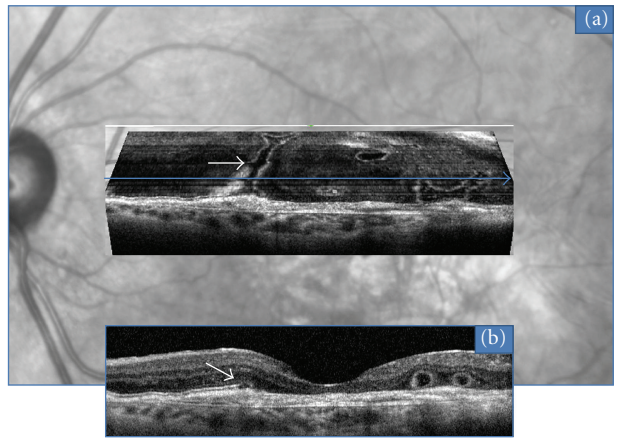

Figure 2: Tubular (arrows) pattern of ORT located above a fibrovascular scar, observed with "en face" OCT (a). Corresponding B-scan OCT (b).

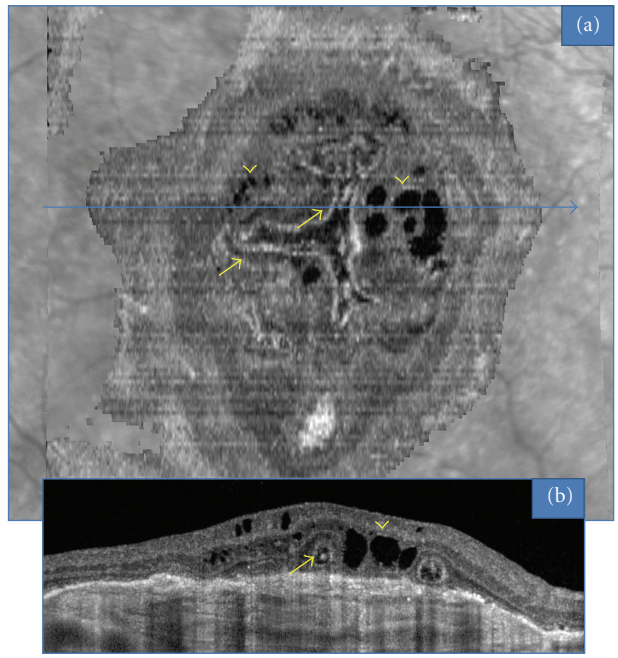

Figure 3: ORT (arrows) associated with intraretinal cystoid cavities (arrow heads) in the case of a fibro-vascular scar, observed with "en face" OCT (a). Corresponding B-scan OCT (b).

Of the 3 eyes with "mixed" AMD, with a fibrotic and atrophic scar, one eye had cystoid lesions and invagination of the ORT network inside the atrophic area.

4. Discussion

The present study describes en-face OCT features of outer retinal tubulations in wet and dry AMD. In this small series, most of the exudative AMD patients with ORT exhibit a similar branching pattern resembling a dendritic cell that we called therefore "pseudodendritic". In atrophic AMD cases, ORTs also exhibit a common pattern around the margin of the atrophic zone, that we called "perilesional."

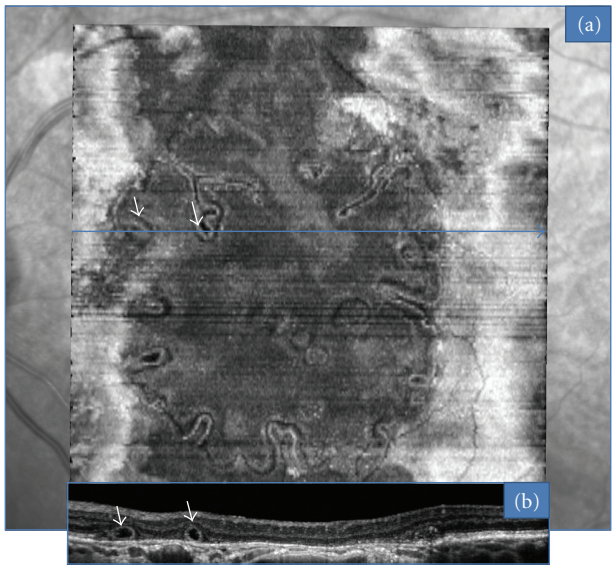

Figure 4: ORT observed with "en face" OCT in a case of geographic atrophy (a). ORTs follow a circular pattern associated with invaginations (arrows) inside the atrophic zone. Corresponding B-scan OCT (b).

"En face" OCT imaging is a technique that has been used for almost ten years [2] although it still has limited application in AMD. Nonetheless, this technique enables to assess the extent of structural damage occurring in AMD. The observation of ORTs, using "en face" OCT, also indicates the size of these lesions inside the retina. ORT can be frequently found among AMD patients (56% of exudative and 21% of atrophic forms) [3], and their incidence is probably underestimated [4]. A combination of SD-OCT with "en face" OCT enhances its sensitivity, allowing earlier diagnosis and a more reliable followup. This technique also improves the distinction between ORT and their main differential diagnosis: cystoid cavities and forms of serous retinal detachments.

Physiopathogenic mechanisms leading to ORT remain poorly understood. According to Zweifel et al. [1], these lesions may result from the outward folding of the photoreceptor layer. Tissue damage associated with retinal degeneration may produce a loss of interdigitations of the photoreceptors with the retinal pigmentary epithelium, and a disruption of tight junctions between the outer segments and adjacent glial elements. Upon repeated microscopic injury, the photoreceptor layer may fold into tubular structures limited to the outer retina.

This type of degeneration is not limited to AMD. ORT have been observed in other degenerative retinal diseases, including Bietti's crystalline dystrophy [5] and Best's disease. Moreover, they have been histologically described under the term "rosette formations" in retinitis pigmentosa [6]. We had previously ventured the hypothesis of an inflammatory origin explaining ORT formation [3]. It now seems unlikely considering the extent of these lesions when viewed by "en face" OCT. The configuration of ORT observed in neovascular (pseudo-dendritic) and atrophic (perilesional) AMD strongly supports the mechanism of a tissue degeneration process causing remodeling of the outer retinal layers.

5. Conclusion

In conclusion, "en face" OCT is a novel technology offering a deeper insight into the understanding and followup of macular disease. This valuable technique allowed the characterization of the main subtypes of tubular formations in AMD: "pseudo-dendritic" forms that develop next to fibrotic scars and "perilesional" forms that develop in the periphery of atrophic areas. This prospective study was based on a limited number of cases. Further studies including more patients are necessary to confirm these results.

Disclosure

No external grants or funds were received in support of this study. None of the authors have a proprietary interest in any of the instruments or procedures used in this study.

References

[1] S. A. Zweifel, M. Engelbert, K. Laud, R. Margolis, R. F. Spaide, and K. B. Freund, "Outer retinal tubulation a novel optical coherence tomography finding," *Archives of Ophthalmology*, vol. 127, no. 12, pp. 1596–1602, 2009.

[2] A. G. Podoleanu, G. M. Dobre, D. J. Webb, and D. A. Jackson, "Simultaneous en-face imaging of two layers in the human retina by low-coherence reflectometry," *Optics Letters*, vol. 22, no. 13, pp. 1039–1041, 1997.

[3] B. Wolff, M. Q. E. Maftouhi, A. Mateo-Montoya, J. A. Sahel, and M. Mauget-Faÿsse, "Outer retinal cysts in age-related macular degeneration," *Acta Ophthalmologica*, vol. 89, no. 6, pp. e496–e499, 2011.

[4] M. Q. E. Maftouhi, B. Wolff, and M. Mauget-Faÿsse, "Outer retinal cysts in exudative age-related macular degeneration: a spectral domain OCT study," *Journal Francais d'Ophtalmologie*, vol. 33, no. 9, pp. 605–609, 2010.

[5] L. A. Yannuzi, "Hereditary chorioretinal dystrophy," in *The Retinal Atlas*, chapter 2, pp. 158–160, Elsevier, New York, NY, USA, 2010.

[6] J. R. Wolter, "A case of advanced retinitis pigmentosa with rosette-shaped formations on the retina.," *Klinische Monatsblätter für Augenheilkunde und für augenärztliche Fortbildung*, vol. 127, no. 6, pp. 687–694, 1955.

Hindawi Publishing Corporation
Journal of Ophthalmology
Volume 2012, Article ID 728457, 6 pages
doi:10.1155/2012/728457

Research Article

Interocular Asymmetry of Foveal Thickness in Parkinson Disease

Eric M. Shrier,[1,2] Christopher R. Adam,[3] Brian Spund,[3] Sofya Glazman,[4] and Ivan Bodis-Wollner[1,2,4]

[1] *Department of Ophthalmology, SUNY Downstate Medical Center, State University of New York, 450 Clarkson Avenue, Brooklyn, NY 11203, USA*
[2] *SUNY Eye Institute, Brooklyn, NY 11023, USA*
[3] *College of Medicine, SUNY Downstate Medical Center, State University of New York, 450 Clarkson Avenue, Brooklyn, NY 11203, USA*
[4] *Department of Neurology, SUNY Downstate Medical Center, State University of New York, 450 Clarkson Avenue, Brooklyn, NY 11203, USA*

Correspondence should be addressed to Ivan Bodis-Wollner, ivan.bodis-wollner@downstate.edu

Received 3 March 2012; Revised 3 June 2012; Accepted 3 June 2012

Academic Editor: Brian Vohnsen

Purpose. To quantify interocular asymmetry (IA) of foveal thickness in Parkinson disease (PD) versus that of controls. *Design*. Prospective case-control series. *Methods*. *In vivo* assessment of foveal thickness of 46 eyes of 23 PD patients and 36 eyes of 18 control subjects was studied using spectral domain optical coherence tomography (SD-OCT). Inner versus outer layer retinal segmentation and macular volumes were quantified using the manufacturer's software, while foveal thickness was measured using the raw data from each eye in a grid covering a 6 by 6 mm area centered on the foveola in 0.25 mm steps. Thickness data were entered into MATLAB software. *Results*. Macular volumes differed significantly at the largest (Zone 3) diameter centered on the foveola (ETDRS protocol). By segmenting inner from outer layers, we found that the IA in PD is mostly due to changes on the slope of the foveal pit at the radial distances of 0.5 and 0.75 mm (1.5 mm and 1 mm diameter). *Conclusions*. About half of the PD patients had IA of the slope of the foveal pit. IA is a potentially useful marker of PD and is expected to be comparable across different SD-OCT equipment. Data of larger groups may be developed in future multicenter studies.

1. Introduction

Parkinson disease (PD) predominantly affects motor functions, but nonmotor deficits in PD have attracted interest as potential diagnostic and treatment biomarkers.

PD patients commonly have subjective visual difficulties that are not well understood. Spectral domain optical coherence tomography (SD-OCT) allows quantification of the thickness of the fovea, the anatomical site of most acute vision, and is emerging as a potential tool in PD [1]. A possible causal link between common visual complaints experienced in PD and retinal dysfunction is supported by the presence of dopaminergic neurons (amacrine cells) [2, 3] of the healthy human adult retina and their impairment in PD [4–6].

In vivo evidence of manifest retinal impairment in PD emanated from a number of retinal electrophysiologic studies, using the pattern electroretinogram (PERG) which suggested that the retina is the most distal source of visual impairment in PD [7–14] (see Supplementary Material 1 available online at doi:10.1155/2012/728457).

SD-OCT retinal scanning is notably fast, readily available, reproducible, noninvasive, and inexpensive as a candidate biomarker. It also supplies a near-histopathologic image of the retina, *in vivo* (see Supplementary Material 2).

Using OCT, it was first shown in 2004 [15] that the nerve fiber layer (NFL) of the retina is thinned in PD. Subsequently retinal thinning in PD was confirmed in most studies [16–19], although details and diagnostic yield differed. There may be several reasons. Most of the studies concentrated

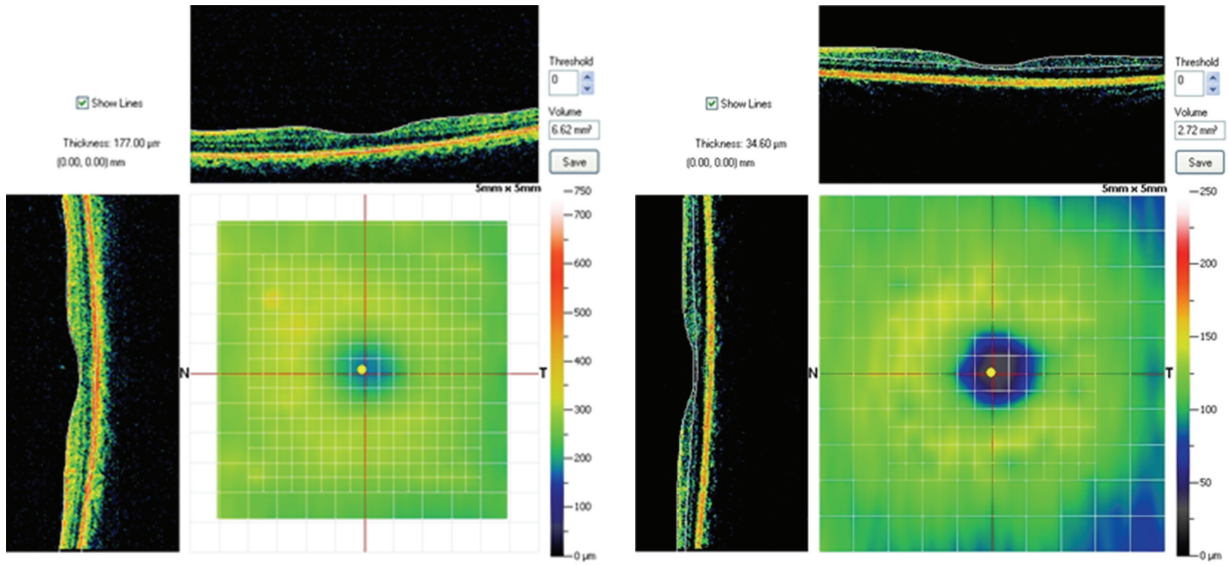

(a) (b)

Figure 1: The central yellow dot in this illustration represents fixation at the foveola. The measuring grid visible in the background is centered on the foveola. Thicknesses at each of the intersecting points of the grid and calculated the volume of each 0.25 × 0.25 mm voxel. (a) shows the SD-OCT profiles through the fovea for a control subject and (b) SD-OCT profile for a PD patient.

on the NFL and not on the inner, cellular retina or they have averaged across the entire fovea and computed total "macular volumes," thereby reducing the likelihood of finding significant differences of diverse retinal layers.

In this study, we concentrated on the foveal pit, where different retinal layers are easier to separate. It is also essential that the comparison control group excluded subjects with presenile dementia and early neurodegenerative conditions, which happen to predominantly occur in the aged. Furthermore, differences exist in the selection of "number of eyes studied versus number of subjects" [20]. Finally, in the statistical analysis of ophthalmic data, one has to account for a correlation between the two eyes [21]. Examination of IA reduces the influence of the natural variation in the thickness of retinal layers. We report significant IA of perifoveolar thickness of the preganglionic retina in PD.

2. Methods

2.1. Subjects. This was a prospective case-control clinical series. The study was approved by the Institutional Review Board for Human Subjects Research of SUNY Downstate Medical Center, and the study adheres to the tenets of the Declaration of Helsinki. Both groups were examined using identical comprehensive neurological and ophthalmological examinations (see Supplementary Material 3). All subjects had best-corrected Snellen visual acuity better than 20/30. There were 46 PD eyes (23 patients) and 36 consecutive age-matched control eyes (18 subjects). PD patients were diagnosed based on the UK Brain Criteria [23]. They were staged using the Hoehn and Yahr (H-Y) [24] criteria and scored according to the standardized clinical tests of UPDRS. The mean ages of PD patients and of healthy subjects were 64.6 ± 7.5 (SD) versus 61.5 ± 9.0 years ($P = 0.77$). The mean H-Y stage was 3.2 (range 1–4) for PD subjects.

As defined by the makers of the SD-OCT software, the measurement of the inner retinal layer (IRL) includes internal limiting membrane (ILM), nerve fiber layer (NFL), ganglion cell layer (GCL), and inner plexiform layer (IPL). Amacrine cells, including dopaminergic amacrine cells, are located in the inner nuclear layer at the border of the IPL. The outer retinal layer (ORL) includes layers from the inner nuclear layer, Henle's fiber layer (HF), outer nuclear layer (ONL), inner (IS) and outer (OS) segments of the photoreceptors up to the retinal pigment epithelium (RPE). full retinal thickness (FRT) is measured from the ILM to the RPE.

2.2. OCT Methodology. Participants were scanned with high resolution SD-OCT (RTVue Model RT 100 (Optovue, Inc.; Fremont, CA)). Grids of 5 × 5 mm (MM5 scan protocol) or 6 × 6 mm (EMM5 scan protocol) are automatically placed to depict, map, and measure sections of the retina. The grids are centered on the area of visual fixation, the foveola (yellow dot) (see Figure 1(a) (control) and Figure 1(b) (PD)). Centration, apparent registration of each scan, and the qualitative regularity of automatically applied segmentation lines were checked for each scan. The program automatically segments inner and outer retinal layers, applies three lines, and quantitative data is then internally computed to yield inner and outer retinal layer and full-thickness retinal measurements. The corresponding numerical data is then exported for statistical analysis.

We manually placed the cursor at each of the intersecting points of the grid and calculated the volume of each 0.25 × 0.25 voxel by the data provided in the OCT equipment.

This (mathematically) yields a matrix of 401 elements per eye studied. Only scans that are of sufficient quality (signal strength = 75% of maximal strength, absent unwanted imaging artifacts, or distortions) were accepted. Images obtained when the vertical and horizontal scans were displaced by more than one voxel (0.25 mm) were rejected.

Macular volumes were quantified using the software of the manufacturer based on the ETDRS protocol. These values are taken off from the automated program of the RT-Vue. They allowed a comparison for foveal thickness and three retinal volumes centered on the foveola with radii of 0.5, 1.5, and 3 mm.

Quantifying segmented foveal thickness: based on the results of our prior study [1] we examined interocular, within-subject variability of the perifoveal area in PD. Inner retinal thickness was measured from the ILM up to and including the boundary interface of the IPL and INL. We exported the corresponding OCT data (images were not manipulated) into MATLAB.

2.3. OCT Interocular Difference (IA), Statistical Analysis. The statistical analysis was performed for both macular volume and segmented retinal thickness (inner versus outer). All statistical analyses were performed using PASW release number 19. The general linear model for repeated measures was used to test for main effect differences between the control and Parkinsonian groups, race, changes over foveal zones, and the interaction of group by foveal zones. Mauchly's test for sphericity was significant indicating a violation of equality of variances between the interocular differences over foveal zones. The Greenhouse-Geisser correction was applied to correct for this violation. For comparing IA at distinct perifoveolar radial distances, the thickness difference for each corresponding voxel was calculated for the four cardinal directions between the left and the right eyes of each subject.

3. Results

3.1. Foveal Thickness and Macular Volumes. Central foveal thickness (0 mm distance = foveola) was the same for PD subjects and controls. There was no effect for group ($F = 0.07$, $P = 0.79$) or for interaction of group by race ($F = 0.78$, $P = 0.47$).

There was significant difference ($F = 4.32$, $P = 0.046$) between the groups in macular volume over the largest diameter (Zone 3 of the ETDRS protocol) (see Figure 2).

This difference in total macular volume is consistent with the results reported by Altintas et al. [16]. There was no effect for the difference between races ($F = 0.341$, $P = 0.713$) or group by race ($F = 0.144$, $P = 0.87$). After correction, there was no significant difference for changes in foveal zone ($F = 1.55$, $P = 0.22$) or the interaction of foveal zone by group ($F = 2.38$, $P = 0.13$).

3.2. Segmented IRL Thickness Measurements. the absolute value of the interocular difference (IOD) was calculated for each control subject and PD patient for each measured radial distance from the foveola. In the PD group, mean

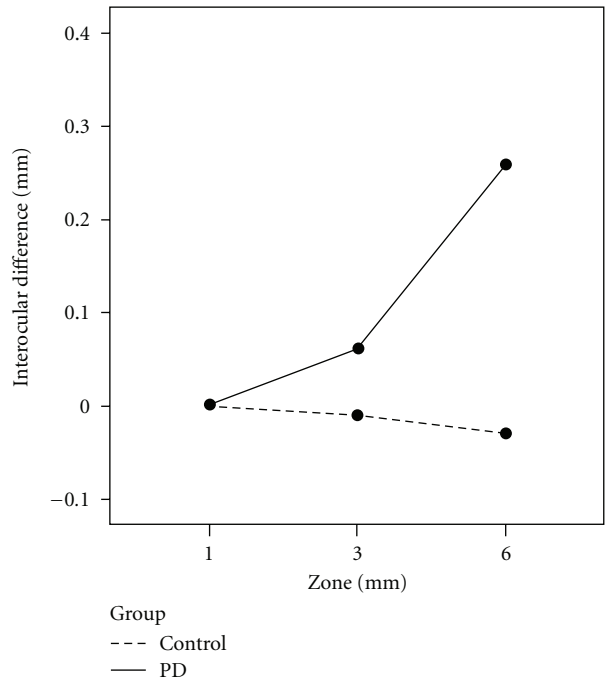

Figure 2: This figure shows interocular asymmetry in the average macular volume measured in the three "standard" (ETDRS) perifoveal zones. The difference increases with zone diameter (5 mm) and reaches statistical significance only when the total macular volume (Zone 3) is compared (see Methods) between PD and control subjects.

IOD reached 12.26 microns at 1.00 mm perifoveolar radius, while, at the corresponding distance controls had a mean 6.97 micron IOD. The mean IOD by group and 1 SD for each distance in controls are shown in Table 1.

At each radial distance, every eye's IA in the four directional quadrants was averaged, and a mean quadratic thickness value was obtained.

The number and percentage of control subjects whose interocular difference was greater than control means at 1 SD are shown in Table 2. Tables 3 and 4 depict the same derived measures for 1.5 and 2 SD.

The tables show that the highest number of patients can be best distinguished at 0.5 and 0.75 mm radial distance. Table 5 represents the grouped data points for 0.5 and 0.75 mm at 1 SD in a predictive-value plot. The inner retina at this particular distance contains some ganglion cells and mostly inner plexiform elements. It represents the zone of the foveal slope, where ganglion cells begin to emerge (see Figure 3). A second flatter "peak" may be present at 1.75 to 2 mm radial distance where ganglion cells and the NFL begin to make a dominant contribution (see Figure 3, after Provis and Hendrickson) [22] to retinal thickness.

Apparently both foveal slope architecture and ganglion cell thickness contribute to deviant IA in PD. By taking 1.5 SD as the criterion, we find that as a population PD patients show significant interocular difference only at radial distances of 0.5, 0.75, and 1 mm from the foveola. Interestingly,

Table 1: Interocular thickness difference (microns) and SDs (1, 1.5, and 2) by radial distance location (mm from foveola) in PD patients and controls.

	0.25 (mm)	0.5 (mm)	0.75 (mm)	1.0 (mm)	1.25 (mm)	1.5 (mm)	1.75 (mm)	2.0 (mm)
Control (mean)	5.50	6.20	5.53	6.97	6.61	7.23	6.32	5.71
PD (mean)	5.11	8.54	10.17	12.26	11.92	10.49	9.76	9.77
Control 1 SD	4.90	4.83	5.54	7.39	8.82	8.69	6.66	6.65
Control 1.5 SD	7.35	7.24	8.32	11.08	13.24	13.04	9.99	9.97
Control 2 SD	9.80	9.66	11.09	14.78	17.66	17.39	13.32	13.30

Table 2: Individual subjects outside their group's retinal thickness mean IOD at 1 control SD at each radial distance (mm). It is evident that the most false positives (controls) were at 1 and 1.25 mm. The highest percentage of correctly identified patients was at 0.5 and 0.75 and to a lesser extent at 1 mm and 1.75 perifoveolar distance (see also Table 5).

	0.25 (mm)	0.5 (mm)	0.75 (mm)	1.0 (mm)	1.25 (mm)	1.5 (mm)	1.75 (mm)	2.0 (mm)
Number of Ctrl	2	1	0	1	2	3	1	1
Number of PD	0	4	5	3	2	3	4	1
Percentage of 23 PD patients	0	17.4	21.7	13	8.7	13	17	4.3
Percentage of 18 controls	11.1	5.5	0	5.5	11.1	16.7	5.5	5.5

this corresponds to the slope of the foveal pit. For a 2 SD criterion, however, there is little IOD. Figure 4 shows the mean interocular difference for all control subjects.

4. Discussion

PD patients have greater IOD in retinal thickness than controls. There appears to be an important difference corresponding to the foveal pit in PD. In the foveal pit, inner but not full-foveal thickness seems to discriminate between PD and controls. Furthermore, interocular symmetry of retinal thickness varies with perifoveolar distance in the fovea in PD. IA appears most evident (see Figure 2) at some distance from the foveola at the slope of the foveal pit where ganglion cells are still scarce [19]. Neither our data nor previous evidence suggests that race, gender, age, and axial length have significant effect on IA of the foveal pit (see Supplementary Material 4). Measuring average macular volume, easy to execute on all OCT models, includes all the inner and outer retinal layers. The distance at 0.75 mm defines a diameter of 1.5 mm. For this diameter, the ETDRS volume did not discriminate between PD and controls. It is likely that the difference for the volumetric measure was not significant as the volume included other regions, closer to the foveola, and outer retinal layers. Our results suggest that therefore macular volumes need to be treated with caution since pathology (as occurs in PD) may not equally affect diverse layers in the foveal pit.

In studies of eye disorders, it is important to consider, for statistical comparison and diagnostic yield, the number of eyes versus the number of subjects [20, 21]. If the correlation between studied variables in the two eyes is high (when within subject variability is low), then it would be permissible, in a large population to use one eye data only. However, a perfect correlation depends on the measure selected. For instance, the interocular correlation of diurnal variation and intraocular pressure (IOP) [25] are highly similar in the two eyes of subjects; however, the coefficients of determination for single pairs range from 0.311 to 0.741. We recommend evaluating each eye of each patient in PD. A clinical advantage of quantifying interocular symmetry is that it is less dependent on absolute thickness measurements and thus less dependent on equipment differences [26].

Motor asymmetry is part of the criteria for clinical and imaging [27, 28] diagnosis of PD. If a patient exhibits symmetrical motor findings, the diagnosis of PD must necessarily be questioned. Although motor asymmetry is clinically well accepted, the reasons for this asymmetry are not well understood [29]. It was suggested that asymmetry is a random process, while dominant handedness [30] is associated with motor asymmetry. Eye dominance and interocular asymmetry in PD have not been evaluated. As the neurosensory retina is impacted in PD, it is plausible that the earliest changes are also asymmetrical and that an area of specificity for the disease would vary amongst a person's eyes. It would thusly be useful as a screening tool and marker of disease presence and progression.

In the search for a quantitative ophthalmological tool to be used as a biomarker for PD (i.e., SD-OCT), a larger normative database is needed. Neurodegenerative diseases increase with age and a number of them have been shown to affect the retina. Both our patients and controls were selected based on identical and rigorous ophthalmological and neurological in- and exclusion criteria (see Supplementary Table 1). We are not aware of any relevant published OCT study in which controls would have been thoroughly screened for neurological conditions. In the future, multivariate analysis may be useful for relaxing the strict criteria to include patients with common conditions such as diabetes mellitus, for instance, who were excluded in the present study.

5. Conclusions

We demonstrate that IA measured at certain radial perifoveal distance may provide help in discriminating between normal and PD subjects. This discrimination affected only

Table 3: Individual subjects outside their group's retinal thickness mean IOD at 1.5 control SD at each radial distance (mm).

	0.25 (mm)	0.5 (mm)	0.75 (mm)	1.0 (mm)	1.25 (mm)	1.5 (mm)	1.75 (mm)	2.0 (mm)
Number of Ctrl	0	0	0	0	1	2	1	1
Number of PD	0	2	4	1	2	2	1	0
Percentage of 23 PD patients	0	8.7	17.4	5.6	8.7	8.7	5.6	0
Percentage of 18 controls	0	0	0	0	5.5	11.1	5.5	5.5

At the stricter (1.5 SD) criterion, 0.75 mm remains as the optimal distance for discriminating PD and controls (compare this table to Tables 1 and 2).

Table 4: Individual subjects outside their group's retinal thickness mean IOD at 2 control SD at each radial distance (mm).

	0.25 (mm)	0.5 (mm)	0.75 (mm)	1.0 (mm)	1.25 (mm)	1.5 (mm)	1.75 (mm)	2.0 (mm)
Number of Ctrl	0	0	0	0	1	0	1	1
Number of PD	0	1	1	1	1	1	1	0
Percentage of 23 PD patients	0	4.3	4.3	4.3	4.3	4.3	4.3	0
Percentage of 18 controls	0	0	0	0	5.5	0	5.5	5.5

Table 5: Predictive value table for grouped data points at 0.5 and 0.75 mm radial distance (1 SD).

		Significant IOD	
		−	+
PD	−	98.2 %	2.8 %
	+	80.4 %	19.6 %

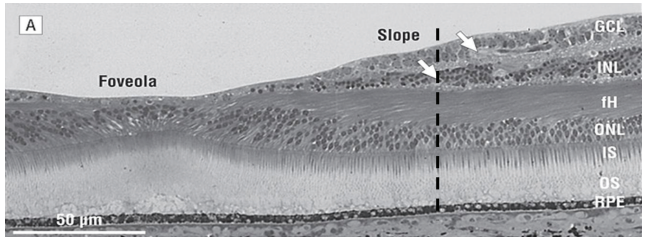

Figure 3: This shows histology of the human retina (after Provis and Hendrickson). Interrupted lines represent perifoveolar radial distances of 0.9 and 1.25 mm where ganglion cells begin to dominate inner retinal thickness. Maximal IA occurs at distances less than 0.9 mm [22].

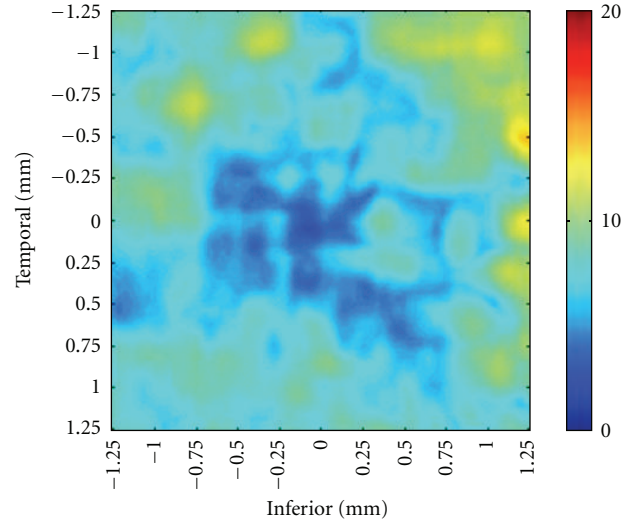

Figure 4: The mean interocular difference map of all control subjects is depicted. Thickness measurements of the inner retina over the central grid of 2.5 × 2.5 mm were obtained, digitally reconstructed, and color-coded. Temporal side is on the left and nasal retina on the right side. Left eyes were reflected horizontally so that the temporal retina is directionally left and the nasal retina is directionally right.

about 1 out of five patients, but the specificity is high. Discrimination appears to be optimal at perifoveal distances of 0.5 and 0.75 mm. This distance corresponds to a region on the slope of the foveal pit where the ganglion cells just begin to emerge. A second flatter "peak" could be present at 2 mm radial distance where ganglion cells and the NFL begin to make a dominant contribution to retinal thickness. Apparently both foveal slope architecture and ganglion cell thickness contribute to deviant IA in PD. IA of the foveal shape has a high specificity and may be a potentially useful marker for PD and may be useful in large multicenter clinical trials.

Authors' Contribution

I. Bodis-Wollner was responsible for the design of the study. E. M. Shrier, C. R. Adam, B. Spund, S. Glazman, and I. Bodis-Wollner conducted the study. All the authors approved the paper.

Acknowledgments

The authors acknowledge the support of NIH/NINDS, Michael J. Fox Foundation (no. 53947), and National Parkinson's Foundation Grant no. 55376. IRB approval was prospective (SUNY Downstate, UMC, Brooklyn, NY).

Informed consent was obtained. Study was HIPAA compliant. Dr. M. Avitable of SUNY Downstate Academic Computing provided statistical support. Drs. T. Liu, I. Selesnick, and Y. Ding of the Department of Electrical Engineering, Polytechnic Institute of NYU, also provided statistical support.

References

[1] M. E. Hajee, W. F. March, D. R. Lazzaro et al., "Inner retinal layer thinning in Parkinson disease," *Archives of Ophthalmology*, vol. 127, no. 6, pp. 737–741, 2009.

[2] J. M. Frederick, M. E. Rayborn, and A. M. Laties, "Dopaminergic neurons in the human retina," *Journal of Comparative Neurology*, vol. 210, no. 1, pp. 65–79, 1982.

[3] P. Witkovsky, "Dopamine and retinal function," *Documenta Ophthalmologica*, vol. 108, no. 1, pp. 17–40, 2004.

[4] J. Nguyen-Legros, "Functional neuroarchitecture of the retina: hypothesis on the dysfunction of retinal dopaminergic circuitry in Parkinson's disease," *Surgical and Radiologic Anatomy*, vol. 10, no. 2, pp. 137–144, 1988.

[5] M. B. A. Djamgoz, M. W. Hankins, J. Hirano, and S. N. Archer, "Neurobiology of retinal dopamine in relation to degenerative states of the tissue," *Vision Research*, vol. 37, no. 24, pp. 3509–3529, 1997.

[6] I. Bodis-Wollner, "Retinopathy in Parkinson disease," *Journal of Neural Transmission*, vol. 116, no. 11, pp. 1493–1501, 2009.

[7] D. J. Brooks, "Functional imaging in relation to parkinsonian syndromes," *Journal of the Neurological Sciences*, vol. 115, no. 1, pp. 1–17, 1993.

[8] I. Gottlob, E. Schneider, W. Heider, and W. Skrandies, "Alteration of visual evoked potentials and electroretinograms in Parkinson's disease," *Electroencephalography and Clinical Neurophysiology*, vol. 66, no. 4, pp. 349–357, 1987.

[9] S. Calzetti, A. Franchi, G. Taratufolo, and E. Groppi, "Simultaneous VEP and PERG investigations in early Parkinson's disease," *Journal of Neurology Neurosurgery and Psychiatry*, vol. 53, no. 2, pp. 114–117, 1990.

[10] H. Ikeda, G. M. Head, and C. J. K. Ellis, "Electrophysiological signs of retinal dopamine deficiency in recently diagnosed Parkinson's disease and a follow up study," *Vision Research*, vol. 34, no. 19, pp. 2629–2638, 1994.

[11] M. Tagliati, I. Bodis-Wollner, and M. Yahr, "The pattern electroretinogram in Parkinson's disease reveals lack of retinal spatial tuning," *Electroenceph and Clin Neurophysiol*, vol. 100, pp. 1–11, 1995.

[12] A. Peppe, P. Stanzione, M. Pierantozzi et al., "Does pattern electroretinogram spatial tuning alteration in Parkinson's disease depend on motor disturbances or retinal dopaminergic loss?" *Electroencephalography and Clinical Neurophysiology*, vol. 106, no. 4, pp. 374–382, 1998.

[13] F. Sartucci, G. Orlandi, C. Lucetti et al., "Changes in pattern electroretinograms to equiluminant red-green and blue-yellow gratings in patients with early Parkinson's disease," *Journal of Clinical Neurophysiology*, vol. 20, no. 5, pp. 375–381, 2003.

[14] M. M. Moschos, G. Tagaris, I. Markopoulos et al., "Morphologic changes and functional retinal impairment in patients with Parkinson disease without visual loss," *European Journal of Ophthalmology*, vol. 21, no. 1, pp. 24–29, 2011.

[15] R. Inzelberg, J. A. Ramirez, P. Nisipeanu, and A. Ophir, "Retinal nerve fiber layer thinning in Parkinson disease," *Vision Research*, vol. 44, no. 24, pp. 2793–2797, 2004.

[16] O. Altintas, P. Iseri, B. Ozkan, and Y. Caglar, "Correlation between retinal morphological and functional findings and clinical severity in Parkinsons Disease," *Documenta Ophthal*, vol. 1116, pp. 137–146, 2008.

[17] G. D. Aaker, J. S. Myung, J. R. Ehrlich, M. Mohammed, C. Henchcliffe, and S. Kiss, "Detection of retinal changes in Parkinson's disease with spectral-domain optical coherence tomography," *Clinical Ophthalmology*, vol. 4, no. 1, pp. 1427–1432, 2010.

[18] C. la Morgia, M. Carbonelli, P. Barboni et al., "Age-related temporal loss of retinal nerve fibers in Parkinson disease: a mitochondrial pattern?" *Investigative Ophthalmology & Visual Science*, vol. 52, 2011, E-Abstract 2984.

[19] I. Bodis-Wollner, B. Spund, T. Liu et al., "Remodeling of the fovea in Parkinson disease," *Investigative Ophthalmology & Visual Science*, vol. 52, 2011, E-Abstract 6660.

[20] F. Ederer, "Shall we count numbers of eyes or numbers of subjects?" *Archives of Ophthalmology*, vol. 89, no. 1, pp. 1–2, 1973.

[21] W. A. Ray and D. M. O'Day, "Statistical analysis of multi-eye data in ophthalmic research," *Investigative Ophthalmology & Visual Science*, vol. 26, no. 8, pp. 1186–1188, 1985.

[22] J. M. Provis and A. E. Hendrickson, "The foveal avascular region of developing human retina," *Archives of Ophthalmology*, vol. 126, no. 4, pp. 507–511, 2008.

[23] A. J. Hughes, S. E. Daniel, L. Kilford, and A. J. Lees, "Accuracy of clinical diagnosis of idiopathic Parkinson's disease: a clinico-pathological study of 100 cases," *Journal of Neurology Neurosurgery and Psychiatry*, vol. 55, no. 3, pp. 181–184, 1992.

[24] M. M. Hoehn and M. D. Yahr, "Parkinsonism: onset, progression and mortality," *Neurology*, vol. 17, no. 5, pp. 427–442, 1967.

[25] J. H. K. Liu, A. J. Sit, and R. N. Weinreb, "Variation of 24-hour intraocular pressure in healthy individuals: right eye versus left eye," *Ophthalmology*, vol. 112, no. 10, pp. 1670–1675, 2005.

[26] G. M. Watson, J. L. Keltner, E. K. Chin, D. Harvey, A. Nguyen, and S. S. Park, "Comparison of retinal nerve fiber layer and central macular thickness measurements among five different optical coherence tomography instruments in patients with multiple sclerosis and optic neuritis," *Journal of Neuro-Ophthalmology*, vol. 31, no. 2, pp. 110–116, 2011.

[27] M. Y. Neuroimaging, *Parkinson's Disease Encyclopedia of Movement Disorders*, 2010.

[28] N. I. Bohnen, S. Minoshima, B. Giordani, K. A. Frey, and D. E. Kuhl, "Motor correlates of occipital glucose hypometabolism in parkinson's disease without dementia," *Neurology*, vol. 52, no. 3, pp. 541–546, 1999.

[29] R. Djaldetti, I. Ziv, and E. Melamed, "The mystery of motor asymmetry in Parkinson's disease," *The Lancet Neurology*, vol. 5, no. 9, pp. 796–802, 2006.

[30] R. J. Uitti, Y. Baba, Z. K. Wszolek, J. D. Putzke, and N. R. Whaley, "Parkinson disease: handedness predicts asymmetry," *Neurology*, vol. 64, no. 11, pp. 1925–1930, 2005.

Hindawi Publishing Corporation
Journal of Ophthalmology
Volume 2012, Article ID 876472, 7 pages
doi:10.1155/2012/876472

Review Article

Spectral Domain Optical Coherence Tomography in the Diagnosis and Management of Vitreoretinal Interface Pathologies

Yoreh Barak, Mark A. Ihnen, and Shlomit Schaal

Department of Ophthalmology and Visual Sciences, University of Louisville School of Medicine, Kentucky Lions Eye Institute, 301 East Muhammad Ali Boulevard, Louisville, KY 40202, USA

Correspondence should be addressed to Shlomit Schaal, s.schaal@louisville.edu

Received 3 February 2012; Revised 19 March 2012; Accepted 5 April 2012

Academic Editor: Stacey S. Choi

The introduction of spectral domain optical coherence tomography (SD-OCT) has enhanced Vitreoretinal Interface (VRI) imaging considerably and facilitated the diagnosis, followup, prognosis determination, and management of VRI-associated pathologies. HR-OCT became a common practical tool seen in almost every ophthalmology practice. Knowledge of SD-OCT image interpretation and recognition of pathologies are required for all ophthalmologists. This paper methodically reviews the normal aging process of the VRI and discusses several commonly encountered VRI pathologies. The role of SD-OCT imaging in VRI-associated disorders such as posterior vitreous detachment, vitreomacular traction syndrome, idiopathic epiretinal membranes, lamellar holes, pseudoholes, and full thickness macular holes is portrayed. Future perspectives of new OCT technologies based on SD-OCT are discussed.

1. The Vitreoretinal Interface

The vitreoretinal interface (VRI) is a complex composite structure connecting the vitreous cortex and the inner retina as illustrated in Figure 1.

The posterior vitreous cortex is 100 μm thick. It consists of densely packed collagen fibrils [1] that insert superficially into the internal limiting membrane (ILM) of the retina [2] and attach to the ILM by glue-like macromolecules, such as laminin, fibronectin, chondroitin, and heparan sulphate proteoglycans [3]. The strongest vitreoretinal adhesions have been described at the optic disc, over the retinal blood vessels and at the macular area [3]. This intimate relationship between cortical vitreous and the retina triggers many of the frequently encountered macular pathologies.

Aging of the human vitreous is characterized by gel liquefaction and the development of fluid-filled pockets, typically beginning in front of the macula and in the central vitreous cavity [4] This progressive process may begin as early as the second decade and eventually leads to degeneration of the vitreous gel and weakened vitreoretinal adhesion. As the collagen-hyaluronate complexes composing the vitreous progressively degenerate, liquefied vitreous pockets enlarge and enter the posterior hyaloid space. Collapse of the vitreous gel, known as syneresis, leads to a complete PVD with time [2].

Optical coherence tomography (OCT), introduced in the 1990's, is a noninvasive in vivo ophthalmic imaging technique [5]. OCT is based on the principal of Michelson interferometry [6]. Interference patterns produced by low coherence light reflected from ocular tissues are processed into an "A-scan" signal. Multiple A-scan signals are aligned to produce a "B-scan" two-dimensional image that can be thought of as a form of "in vivo histology [6]." In 2002, the time-domain OCT, which was based on a moving reference mirror, became commercially available with an axial resolution of 10 μm.

Since 2004, higher resolution spectral-domain OCT (SD-OCT) has entered clinical ophthalmic practice. SD-OCT is not limited by moving parts. SD-OCT relies on a spectrometer and high-speed camera using the mathematical premise of Fourier transformation for analysis of the reflected light. This results in a significant increase in the amount of data

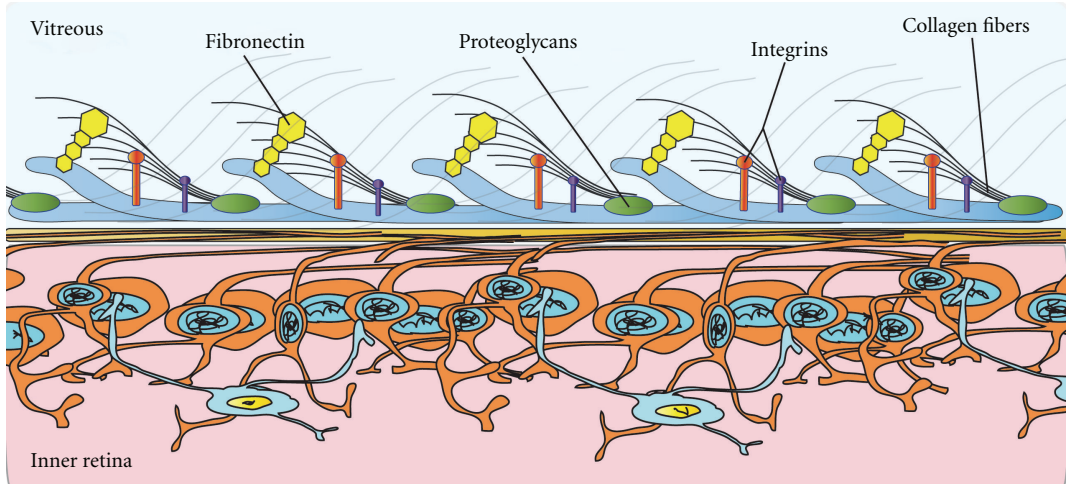

Figure 1: Illustration of the vitreoretinal attachments at the vitreoretinal interface. The posterior vitreous cortex is attached to the ILM by collagen fibers at the vitreoretinal interface. These fibers fuse with the ILM and along with macromolecules, such as laminin, fibronectin, and chondroitin anchor the vitreous cortex to the retina.

acquired during each session while reducing motion artifacts with an increased signal-to-noise ratio when compared with time-domain OCT. Commercial available SD-OCT machines have a reported axial resolution of 5 to 7 microns [7]. There are some prototypes achieving 3 microns of axial resolution [7].

This cross-sectional imaging technology has allowed investigators to study and manage patients with VRI disease processes that were previously unrecognizable by biomicroscopy alone. OCT was the primary contributor to our understanding of the pathogenesis and the anatomical sequence of events that underlie VRI pathologies. This revolutionary imaging modality is now prevalent in all ophthalmology clinic settings as it greatly enhances physicians' ability to recognize and diagnose VRI pathologies. This paper reviews the uses of SD-OCT in the evaluation, followup, and management of VRI-associated disorders such as posterior vitreous detachment, vitreomacular traction syndrome, idiopathic epiretinal membranes, lamellar holes, pseudoholes, and full thickness macular holes as illustrated in Figure 2.

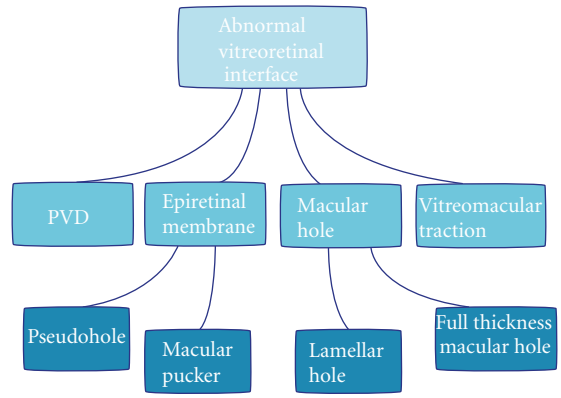

Figure 2: Vitreoretinal-interface-associated pathologies.

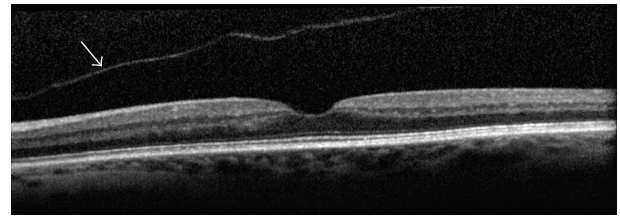

Figure 3: Posterior vitreous detachment (arrow).

2. Posterior Vitreous Detachment

Posterior vitreous detachment (PVD) is defined as a separation between the posterior vitreous cortex and the ILM of the retina (Figure 3).

Aging of the vitreous and syneresis leads to a complete PVD with time [2]. The most commonly associated clinical symptom is the development of floaters. With aging, complete PVD becomes more common with a 10% prevalence in people under the age of 50 and up to 63% of people over the age of 70 [8]. The most common complications of PVD are retinal tears, vitreous hemorrhage, rhegmatogenous retinal detachment, and retinal or optic disc hemorrhage [2, 6, 9]. These complications are mainly caused by dynamic vitreous traction on focal areas of firm vitreoretinal adhesion [9].

For many years PVD could only be diagnosed clinically using biomicroscopy and was believed to be an acute event. Subsequently, ultrasonography was used as the main imaging modality for documentation of PVD [2]. Despite its relatively gross resolution (1 mm) it is nonetheless a reliable tool to determine the presence of a PVD [10]. It is indeed advantageous in eyes with media opacities such as corneal opacities, dense cataracts, vitreous hemorrhage, or vitreous inflammation.

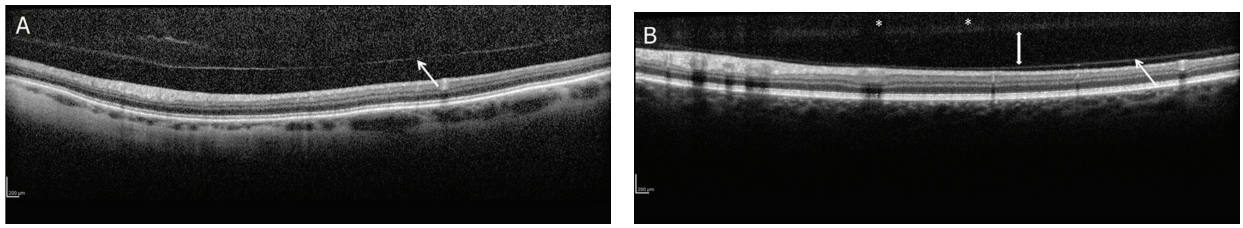

(a) (b)

Figure 4: SD-OCT images of PVD and vitreoschisis. PVD; posterior hyaloid (arrow) separated from the retina (a). Vitreoschisis with liquefaction (double-head arrow) of the vitreous between a formed vitreous (asterisk) and an attached posterior hyaloid (arrow).

SD-OCT enables us, in our day-to-day practice, to image and to study the posterior hyaloid face and its intimate relationship with the retina. It allows not only early diagnosis of vitreous pathologies but also the ability to differentiate PVD from other clinical entities, such as vitreoschisis (Figure 4). The SD-OCT is a reliable and an objective tool to assist the clinician in making the correct diagnosis and determining treatment options. For example, an observation of vitreomacular traction syndrome following an acute traumatic incomplete PVD that was recently demonstrated by SD-OCT may be transient in nature, allowing the option of observation and followup by SD-OCT as an alternative to early surgical intervention [11]. A recent study by Johnson [4] used SD-OCT imaging to evaluate the early stages of PVD. It was revealed that PVD is most probably an insidious, chronic event that begins in the perifoveal macula and progressively detaches over a prolonged period of time, leaving the foveal and optic nerve attachment to separate last.

The majority of PVDs are asymptomatic and do not require any treatment [4]. Most symptomatic patients experience floaters and predominantly do well with observation alone. Although still controversial, there have been a growing number of recent reports advocating small incision sutureless vitrectomy surgery for the removal of symptomatic floaters [12, 13].

Vitreoschisis and incomplete PVD, determined in part by the size and strength of the residual vitreoretinal adhesion [4], may be complicated by a variety of vitreoretinal interface pathologies in the macular area as discussed below.

3. Vitreomacular Traction Syndrome

The classic form of Vitreomacular traction (VMT) syndrome is characterized by partial PVD with residual strong and focal posterior vitreomacular adhesions. This results in anteroposterior and tangential tractional forces applied by the vitreous to the foveal and parafoveal regions. Based on SD-OCT data, it appears that there are 2 subclasses of vitreomacular traction; focal foveolar adhesion and broad macular adhesion [4, 14, 15]. Decreased visual acuity may result from secondary intraretinal edema and a distortion of the normal macular architecture. Other common symptoms associated with VMT syndrome include metamorphopsia, micropsia, and photopsia.

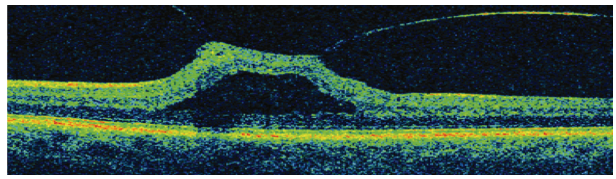

Figure 5: Vitreomacular traction.

Now commercially available, OCT has been tremendously helpful in confirming many cases of VMT that were clinically undetectable (Figure 5). Although conventional time domain OCT was able to demonstrate the vitreoretinal interface, the ability to image the posterior hyaloid membrane was limited by the slow scan speed, limited sensitivity, and poor axial resolution. The increased axial resolution, the augmented signal/noise ratio, and the higher scan rate of new SD-OCT have dramatically improved the ability to visualize the vitreomacular interface and posterior hyaloid membrane [16].

Three-dimensional scans made possible with SD-OCT have advanced the comprehensive evaluation of the vitreoretinal interface providing additional clinically significant information. The 3-dimensional reconstruction modality enables meticulous presurgical planning, with the potential for improved postsurgical outcomes [16]. Koizum et al. [14] performed a three-dimensional evaluation of the VRI in VMT syndrome using SD-OCT. They found that most of the eyes with VMT syndrome had concurrent epiretinal membranes. These epiretinal membranes increase the adhesion between the vitreous and the retina and serve as an anchor for the cortical vitreous on the inner surface of the retina therefore preventing spontaneous separation of the vitreous from the macula.

SD-OCT has triggered focused attention to special conditions in which VRI pathologies develop. For instance, a complete PVD is less prevalent in diabetic patients with clinically significant diabetic macular edema compared to diabetic patients without diabetic macular edema [17]. It is well established that diabetic macular edema may be exacerbated by the vitreomacular traction effects of partial vitreous detachment [18]. A recent study using SD-OCT to assess the VRI in eyes with diabetic macular edema, epiretinal

membranes, and incomplete PVD [19] found that the posterior cortical vitreous and the hyper-reflective adherent membrane, which is generally designated as an epiretinal membrane, appeared as one continuous thick membrane. Based on these novel observations which were supported by histologic findings [20], it can be assumed that the hyperreflective adherent epimacular membrane is commonly composed of an integrated fibrocellular membrane from the epiretinal membraneposterior hyaloid complex.

In daily practice, in addition to confirming the diagnosis of VMT, SD-OCT plays an important role in following patients with VMT and in determining their visual prognosis. In some cases, spontaneous resolution of traction may occur, justifying a period of clinical observation before surgical intervention [21, 22]. For symptomatic patients, small gauge vitrectomy surgery and release of the vitreous traction may be easily and safely applied [23, 24]. It is important to keep in mind that clinical and histologic studies have shown that residual cortical vitreous commonly adheres to the inner retinal surface following vitrectomy despite peeling of the posterior hyaloids [25]. Cortical postoperative vitreous remnants may organize into a fibrocellular epiretinal membrane with subsequent contraction causing macular pucker [26]. Other limitations of vitrectomy include surgical complications such as retinal tears, retinal detachments, cataract formation/progression, and intraocular infection as well as high costs.

Pharmacologic vitreolysis, applied as an intravitreal injection, is an emerging possible treatment for persistent vitreomacular-adhesion-related pathologies [27].

Over the past 15 years, investigators have increasingly examined alternative methods for PVD induction which focused on the use of pharmacologic agents to modify the molecular structure of the vitreous thereby eliminating its role in the pathogenesis of retinal diseases. While early interest in pharmacologic vitreolysis has focused on its application as an adjunct to vitrectomy surgery and removal of fibrovascular proliferative membranes [28], investigators have quickly realized its potential as a stand-alone therapy [29]. Vitreolytic agents may potentially improve anatomical and functional outcomes in VMT patients. They may also be used as a prophylactic measure in conditions in which PVD is associated with an improved prognosis (DME) [27].

Results from an initial clinical trial evaluating the safety and preliminary efficacy of vitreolysis with intravitreal microplasmin in patients suffering from VMT show the drug to be well tolerated and capable of inducing a pharmacologic PVD in some patients [30].

The ancillary benefits of pharmacologic vitreolysis include: decreased costs, based on shorter surgical times or decreased incidence of progressive disease requiring surgery; greater access to therapy, based on the simple instrumentation involved in the injection administration and a possible future transition to office-based procedures [31]. Furthermore, these agents will reduce patient exposure to inherent vitrectomy-related complications, such as endophthalmitis, cataract formation, iatrogenic retinal breaks and anesthesia related complications [27].

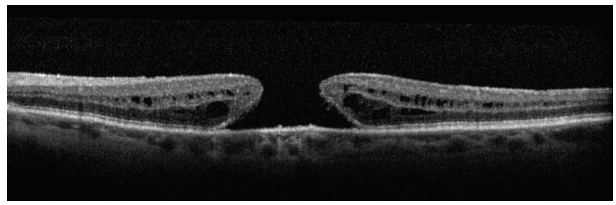

Figure 6: Full thickness macular hole.

4. Full Thickness Macular Hole

Full thickness macular hole (FTMH) is a vertical split in the foveal neurosensory retina (Figure 6). It is more common in females and occurs primarily in the sixth to eighth decades of life. The risk of developing a macular hole in the other eye of patients with unilateral macular hole has been reported to be 11–13% overall [32]; however, it increases to 50% if a premacular hole configuration is noted on OCT [33].

The etiology of macular hole formation is still unknown. SD-OCT data gathered in recent years support the hypothesis that vitreoretinal abnormalities and vitreomacular traction play a major role in idiopathic macular hole formation [32, 34]. Visual symptoms include metamorphopsia and diminished central visual acuity ranging from 20/40 to 5/200 in later stages.

Clinically, a FTMH might be confused with other VRI disorders such as a pseudohole and lamellar hole (discussed below). SD-OCT helps the clinician distinguish between these VRI conditions and has improved our understanding of the role of vitreoretinal adhesions in the pathogenesis of these disorders. The conventional management of FTMH is surgical treatment. Initially advocated in 1991 by Kelly and Wendel [35], vitrectomy with gas tamponade and face down positioning is currently the treatment of choice for FTMH. Variations of this procedure have evolved over the years to include ILM peeling, with or without adjuvant staining [36]. Recent data questions the need for face down positioning after surgery for small ($<400\,\mu$m) FTMH [37, 38]. More recently, pharmacological vitreolysis has been recommended for the closure of small FTMH [30].

In day to day retina clinic, SD-OCT is an invaluable tool in the pre- and postoperative diagnosis and followup of patients with FTMH. Newly, a mathematical analog of the premacular hole foveal anatomic configuration was first described to enable recognition of patients prone to developing FTMH (as seen in Figure 7) [33]. Using OCT foveal thickness maps, the mathematical analog of a premacular hole, foveal anatomic configuration was found to be significantly different from the normal foveal configuration and was composed of a steep nonsymmetrical foveal slope with a wide fovea on OCT scans. Fifty percent of the patients with a premacular hole configuration consequently developed bilateral macular holes. This high incidence compared to a previously reported incidence of 11% to 13% of bilateral macular holes [32] may indicate that this foveal configuration predisposes a subset of high risk patients to develop bilateral macular holes [33]. The exciting new clinical ability to identify this distinct macular configuration may allow

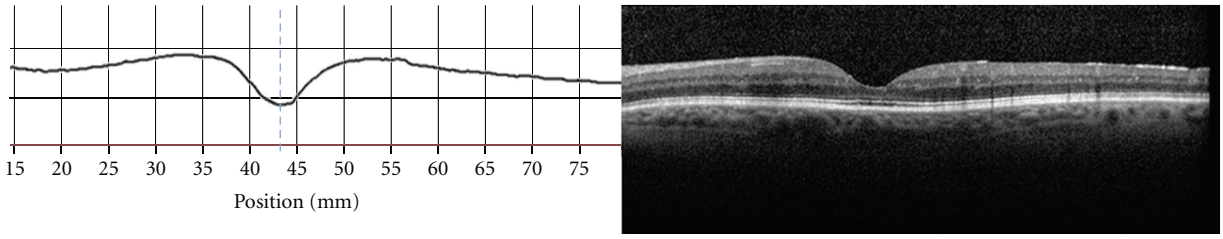

Figure 7: Premacular hole configuration SD-OCT (right) and foveal thickness graph (left) illustrating steep and asymmetrical slopes.

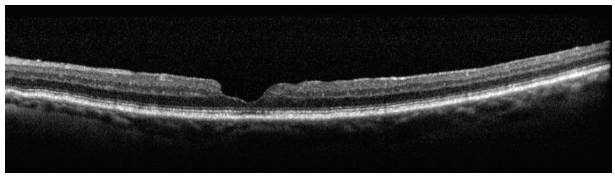

Figure 8: Lamellar hole with intact photoreceptors.

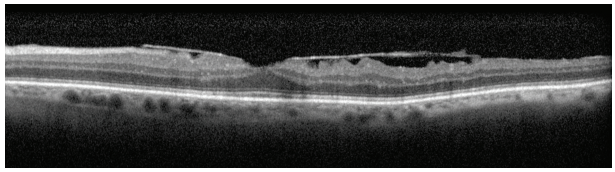

Figure 9: Pseudohole without any neurosensory defects.

early diagnosis, close followup and better management of macular hole-prone patients as seen in Figure 7 [33].

SD-OCT is also used to determine the prognosis for vision recovery by assessing the structural integrity of the photoreceptors before and after macular hole surgery by imaging of the inner segment/outer segment photoreceptor (IS/OS junction) defect in patients with macular holes. The extent of the IS/OS junction defect can be a prognostic feature for the visual outcome after macular hole surgery [39, 40]. A study evaluating the ability of SD-OCT images of the IS/OS junction to predict macular hole surgery outcomes demonstrated that the mean total area and maximum length of the IS/OS junction defect at 12 months after surgery was significantly and negatively correlated with the postoperative visual acuity. The conclusion of the study was that SD-OCT is useful for quantitatively measuring IS/OS junction defects, and that postoperative IS/OS junction may play an important role in visual recovery after macular hole surgery [40].

5. Lamellar Hole

Lamellar hole is a partial thickness defect in the neurosensory retina with intact photoreceptors, as shown in (Figure 8).

6. Pseudohole

Pseudohole is a hole in an epiretinal membrane (ERM) without any neurosensory defects in the retina (Figure 9).

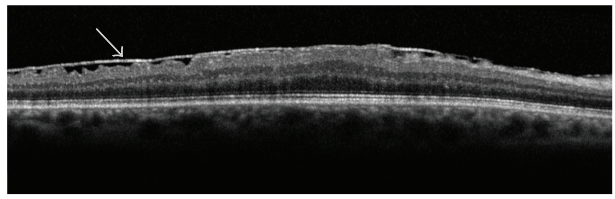

Figure 10: Epiretinal membrane (arrow).

7. Epiretinal Membrane

Epiretinal membrane (ERM) or macular pucker is an avascular, fibrocellular membrane on the inner surface of the retina (Figure 10).

ERM results from proliferative changes at the VRI and can be either secondary to other ocular conditions or idiopathic in nature. Secondary membranes are associated with a variety of retinal disorders, including retinal tears, retinal vascular diseases (branch retinal vein occlusion and central retinal vein occlusion), uveitis, trauma, or retinal detachment surgery [1]. Partial or complete PVD has been found in 80% to 95% of eyes with idiopathic ERM [41]. This was suggested to be secondary to vitreous schisis and vitreous remnants on the retina promoting subsequent epiretinal fibrocellular proliferation [42].

Idiopathic premacular membranes have a wide range of severity. They may be quite subtle, causing minimal loss of vision or may result in macular edema and distorted vision caused by traction exerted by the membrane and resultant leakage from the perifoveal capillaries.

In clinical practice SD-OCT has proven useful in the evaluation and treatment of ERMs. Using SD-OCT, one can easily differentiate the posterior hyaloid, a minimally reflective signal, from an ERM, which is highly reflective [43]. OCT has also been helpful in confirming the relationship between PVD and ERM. OCT is valuable for following the natural history of epiretinal membranes [43]. Visually significant ERMs are usually removed surgically resulting in a 2-line improvement on average [44]. Although surgical intervention was previously advised only after significant reduction in visual acuity (<20/60), SD-OCT made it possible to obtain a very accurate image of early changes in the retina, such as ERM-related macular edema and/or distortion of the inner and outer retina allowing early, minimally invasive, small gauge surgical intervention, and possibly better visual outcome.

8. Future Perspective

New advancements in the use of high-resolution OCT for retinal imaging are continuously emerging. These practical and experimental tools most probably will have a marked impact on the way we treat our patients in retina practice in the future. One of the most intriguing developments is the experimental use of intraoperative microscope-mounted SD-OCT. The possibility to use SD-OCT intraoperatively provides thrilling new insights into the subtle changes of retinal anatomy during the performance of macular surgery. Intra-operative SD-OCT may be a future practical tool for facilitating vitreoretinal surgery [45]. SD-OCT high axial resolution also allows for a three dimensional en face or "C-scan" to be produced offering a new view of the different layers of the retina and the vitreoretinal relationship [7, 46]. Another new development is the Swept source OCT that can achieve ultrahigh axial resolution of 2-3 μm by sweeping a narrow bandwidth light source through a broad optical range [47]. Total retinal blood flow measurement with this newer ultrahigh speed swept source/Fourier domain OCT [47] may enable us to demonstrate and measure the increased blood flow reported after peeling of the posterior hyaloid [48] and may abele us to measure blood flow in occlusive retinal vascular diseases and/or ischemic diseases of the retina.

9. Conclusion

SD-OCT has broadened a new horizon in the basic understanding and interpretation of vitreoretinal interface disorders. It allows early diagnosis, better followup, and more intelligent information-based surgical decision making. SD-OCT has recently been used in the screening of patients at risk for vitreoretinal interface disorders, as well as determining and predicting their visual prognosis. With further advancement of this technology, higher resolution OCT carries the potential of perfecting visual outcomes for patients with VRI disorders.

Disclosure

None of authors have any financial interest to disclosure.

References

[1] J. Sebag, "Anatomy and pathology of the vitreo-retinal interface," *Eye*, vol. 6, no. 6, pp. 541–552, 1992.

[2] M. W. Johnson, "Perifoveal vitreous detachment and its macular complications," *Transactions of the American Ophthalmological Society*, vol. 103, pp. 537–567, 2005.

[3] T. L. Ponsioen, J. M. M. Hooymans, and L. I. Los, "Remodelling of the human vitreous and vitreoretinal interface—a dynamic process," *Progress in Retinal and Eye Research*, vol. 29, no. 6, pp. 580–595, 2010.

[4] M. W. Johnson, "Posterior vitreous detachment: evolution and complications of its early stages," *American Journal of Ophthalmology*, vol. 149, no. 3, pp. 371–e1, 2010.

[5] C. A. Puliafito, M. R. Hee, C. P. Lin et al., "Imaging of macular diseases with optical coherence tomography," *Ophthalmology*, vol. 102, no. 2, pp. 217–229, 1995.

[6] G. J. Jaffe and J. Caprioli, "Optical coherence tomography to detect and manage retinal disease and glaucoma," *American Journal of Ophthalmology*, vol. 137, no. 1, pp. 156–169, 2004.

[7] D. F. Kiernan, W. F. Mieler, and S. M. Hariprasad, "Spectral-domain optical coherence tomography: a comparison of modern high-resolution retinal imaging systems," *American Journal of Ophthalmology*, vol. 149, no. 1, pp. 18–e2, 2010.

[8] R. J. Foos and N. C. Wheeler, "Vitreoretinal juncture. Synchysis senilis and posterior vitreous detachment," *Ophthalmology*, vol. 89, no. 12, pp. 1502–1512, 1982.

[9] M. A. Novak and R. B. Welch, "Complications of acute symptomatic posterior vitreous detachment," *American Journal of Ophthalmology*, vol. 97, no. 3, pp. 308–314, 1984.

[10] N. Kicova, T. Bertelmann, S. Irle, W. Sekundo, and S. Mennel, "Evaluation of a posterior vitreous detachment: a comparison of biomicroscopy, B-scan ultrasonography and optical coherence tomography to surgical findings with chromodissection," *Acta Ophthalmol*, vol. 90, no. 4, pp. e264–e268, 2012.

[11] M. Lorusso, L. M. Ferrari, M. Leozappa, A. P. Modoni, and T. M. Ferrari, "Transient vitreomacular traction syndrome caused by traumatic incomplete posterior vitreous detachment," *European Journal of Ophthalmology*, vol. 21, no. 5, pp. 668–670, 2011.

[12] H. S. Tan, M. Mura, S. Y. Lesnik Oberstein, and H. M. Bijl, "Safety of vitrectomy for floaters," *American Journal of Ophthalmology*, vol. 151, no. 6, pp. 995–998, 2011.

[13] M. Mura, L. A. Engelbrecht, M. D. de Smet et al., "Surgery for floaters," *Ophthalmology*, vol. 118, p. 1894, 2011.

[14] H. Koizumi, R. F. Spaide, Y. L. Fisher, K. B. Freund, J. M. Klancnik, and L. A. Yannuzzi, "Three-Dimensional Evaluation of Vitreomacular Traction and Epiretinal Membrane Using Spectral-Domain Optical Coherence Tomography," *American Journal of Ophthalmology*, vol. 145, no. 3, pp. 509–e1, 2008.

[15] K. Sonmez, A. Capone Jr, M. T. Trese, and G. A. Williams, "Vitreomacular traction syndrome: impact of anatomical configuration on anatomical and visual outcomes," *Retina*, vol. 28, no. 9, pp. 1207–1214, 2008.

[16] S. Wolf and U. Wolf-Schnurrbusch, "Spectral-domain optical coherence tomography use in macular diseases: a review," *Ophthalmologica*, vol. 224, no. 6, pp. 333–340, 2010.

[17] F. P. Nasrallah, A. E. Jalkh, F. Van Coppenolle et al., "The role of the vitreous in diabetic macular edema," *Ophthalmology*, vol. 95, no. 10, pp. 1335–1339, 1988.

[18] M. W. Johnson, "Etiology and Treatment of Macular Edema," *American Journal of Ophthalmology*, vol. 147, no. 1, pp. 11–e1, 2009.

[19] A. Ophir and M. R. Martinez, "Epiretinal membranes and incomplete posterior vitreous detachment in diabetic macular edema, detected by spectral-domain optical coherence tomography," *Investigative Ophthalmology & Visual Science*, vol. 52, pp. 6414–6420, 2011.

[20] A. Gandorfer, M. Rohleder, S. Grosselfinger, C. Haritoglou, M. Ulbig, and A. Kampik, "Epiretinal pathology of diffuse diabetic macular edema associated with vitreomacular traction," *American Journal of Ophthalmology*, vol. 139, no. 4, pp. 638–652, 2005.

[21] D. J. Sulkes, M. S. Ip, C. R. Baumal, H. K. Wu, and C. A. Puliafito, "Spontaneous resolution of vitreomacular traction documented by optical coherence tomography," *Archives of Ophthalmology*, vol. 118, no. 2, pp. 286–287, 2000.

[22] I. Voo, E. C. Mavrofrides, and C. A. Puliafito, "Clinical applications of optical coherence tomography for the diagnosis and management of macular diseases," *Ophthalmology Clinics of North America*, vol. 17, no. 1, pp. 21–31, 2004.

[23] G. Y. Fujii, E. De Juan Jr, M. S. Humayun et al., "A new 25-gauge instrument system for transconjunctival sutureless vitrectomy surgery," *Ophthalmology*, vol. 109, no. 10, pp. 1807–1812, 2002.

[24] O. Sandali, M. El Sanharawi, N. Lecuen et al., "25-, 23-, and 20-gauge vitrectomy in epiretinal membrane surgery: a comparative study of 553 cases," *Graefe's Archive for Clinical and Experimental Ophthalmology*, pp. 1–9, 2011.

[25] K. H. Sonoda, T. Sakamoto, H. Enaida et al., "Residual vitreous cortex after surgical posterior vitreous separation visualized by intravitreous triamcinolone acetonide," *Ophthalmology*, vol. 111, no. 2, pp. 226–230, 2004.

[26] J. Sebag, P. Gupta, R. R. Rosen, P. Garcia, and A. A. Sadun, "Macular holes and macular pucker: the role of vitreoschisis as imaged by optical coherence tomography/scanning laser ophthalmoscopy," *Transactions of the American Ophthalmological Society*, vol. 105, pp. 121–129, 2007.

[27] E. W. Schneider and M. W. Johnson, "Emerging nonsurgical methods for the treatment of vitreomacular adhesion: a review," *Clinical Ophthalmology*, vol. 5, no. 1, pp. 1151–1165, 2011.

[28] L. C. Moorhead and N. Radtke, "Enzyme-assisted vitrectomy with bacterial collagenase: pilot human studies," *Retina*, vol. 5, no. 2, pp. 98–100, 1985.

[29] T. H. Tezel, L. V. Del Priore, and H. J. Kaplan, "Posterior vitreous detachment with dispase," *Retina*, vol. 18, no. 1, pp. 7–15, 1998.

[30] M. D. de Smet, A. Gandorfer, P. Stalmans et al., "Microplasmin intravitreal administration in patients with vitreomacular traction scheduled for vitrectomy. The MIVI I trial," *Ophthalmology*, vol. 116, no. 7, pp. 1349–1355, 2009.

[31] J. Sebag, "Pharmacologic vitreolysis—premise and promise of the first decade," *Retina*, vol. 29, no. 7, pp. 871–874, 2009.

[32] H. Niwa, H. Terasaki, Y. Ito, and Y. Miyake, "Macular hole development in fellow eyes of patients with unilateral macular hole," *American Journal of Ophthalmology*, vol. 140, no. 3, pp. 370–375, 2005.

[33] Y. Barak, M. P. Sherman, and S. Schaal, "Mathematical analysis of specific anatomic foveal configurations predisposing to the formation of macular holes.," *Investigative Ophthalmology & Visual Science*, vol. 52, no. 11, pp. 8266–8270, 2011.

[34] Z. Michalewska, J. Michalewski, B. L. Sikorski et al., "A study of macular hole formation by serial spectral optical coherence tomography," *Clinical and Experimental Ophthalmology*, vol. 37, no. 4, pp. 373–383, 2009.

[35] N. E. Kelly and R. T. Wendel, "Vitreous surgery for idiopathic macular holes: results of a pilot study," *Archives of Ophthalmology*, vol. 109, no. 5, pp. 654–659, 1991.

[36] S. Schaal and C. C. Barr, "Management of macular holes: a comparison of 1-year outcomes of 3 surgical techniques," *Retina*, vol. 29, no. 8, pp. 1091–1096, 2009.

[37] C. A. Lange, L. Membrey, N. Ahmad et al., *Pilot Randomised Controlled Trial of Face-down Positioning Following Macular Hole Surgery*, Eye, London, UK, 2011.

[38] A. Tatham and S. Banerjee, "Face-down posturing after macular hole surgery: a meta-analysis," *British Journal of Ophthalmology*, vol. 94, no. 5, pp. 626–631, 2010.

[39] L. K. Chang, H. Koizumi, and R. F. Spaide, "Disruption of the photoreceptor inner segment-outer segment junction in eyes with macular holes," *Retina*, vol. 28, no. 7, pp. 969–975, 2008.

[40] M. Inoue, Y. Watanabe, A. Arakawa, S. Sato, S. Kobayashi, and K. Kadonosono, "Spectral-domain optical coherence tomography images of inner/outer segment junctions and macular hole surgery outcomes," *Graefe's Archive for Clinical and Experimental Ophthalmology*, vol. 247, no. 3, pp. 325–330, 2009.

[41] S. Kishi and K. Shimizu, "Oval defect in detached posterior hyaloid membrane in idiopathic preretinal macular fibrosis," *American Journal of Ophthalmology*, vol. 118, no. 4, pp. 451–456, 1994.

[42] R. G. Schumann, M. M. Schaumberger, M. Rohleder, C. Haritoglou, A. Kampik, and A. Gandorfer, "Ultrastructure of the vitreomacular interface in full-thickness idiopathic macular holes: a consecutive analysis of 100 cases," *American Journal of Ophthalmology*, vol. 141, no. 6, pp. 1112–e1, 2006.

[43] R. G. Mirza, M. W. Johnson, and L. M. Jampol, "Optical coherence tomography use in evaluation of the vitreoretinal interface: a review," *Survey of Ophthalmology*, vol. 52, no. 4, pp. 397–421, 2007.

[44] J. G. Wong, N. Sachdev, P. E. Beaumont, and A. A. Chang, "Visual outcomes following vitrectomy and peeling of epiretinal membrane," *Clinical and Experimental Ophthalmology*, vol. 33, no. 4, pp. 373–378, 2005.

[45] R. Ray, D. E. Baraano, J. A. Fortun et al., "Intraoperative microscope-mounted spectral domain optical coherence tomography for evaluation of retinal anatomy during macular surgery," *Ophthalmology*, vol. 118, no. 11, pp. 2212–2217, 2011.

[46] M. Alkabes, C. Salinas, L. Vitale, A. Bures-Jelstrup, P. Nucci, and C. Mateo, "En face optical coherence tomography of inner retinal defects after internal limiting membrane peeling for idiopathic macular hole," *Investigative Ophthalmology & Visual Science*, vol. 52, no. 11, pp. 8349–8355, 2011.

[47] B. Baumann, B. Potsaid, M. F. Kraus et al., "Total retinal blood flow measurement with ultrahigh speed swept source/Fourier domain OCT," *Biomedical Optics Express*, vol. 2, no. 6, pp. 1539–1552, 2011.

[48] T. Tezel, S. Schaal, E. Downing, A. Soliman, A. El-Baz, and H. Kaplan, *Vitrectomy with Posterior Hyaloid Peeling Increases Optic Nerve and Retinal Perfusion*, Retina Congress, New York, NY, USA, 2009.

Hindawi Publishing Corporation
Journal of Ophthalmology
Volume 2012, Article ID 107053, 6 pages
doi:10.1155/2012/107053

Clinical Study

Comparison of Retinal Nerve Fiber Layer Thickness Measurements in Healthy Subjects Using Fourier and Time Domain Optical Coherence Tomography

Isabel Pinilla,[1,2] Elena Garcia-Martin,[2,3] Miriam Idoipe,[2,3] Eva Sancho,[2,3] and Isabel Fuertes[2,3]

[1] *Ophthalmology Department, Lozano Blesa University Hospital, c/ San Juan Bosco 15, 50009 Zaragoza, Spain*
[2] *Aragones Institute of Health Science, IIS Aragon, C/ Gómez Laguna 25, 50009 Zaragoza, Spain*
[3] *Ophthalmology Department, Miguel Servet University Hospital, c/ Isabel la Católica 1-3, 50009 Zaragoza, Spain*

Correspondence should be addressed to Isabel Pinilla, ipinilla@unizar.es

Received 3 February 2012; Accepted 6 March 2012

Academic Editor: Robert J. Zawadzki

Purpose. To compare the retinal nerve fiber layer (RNFL) measurements using two different ocular coherence tomography (OCT) devices: Cirrus Fourier domain OCT and Stratus time domain OCT. To analyze reproducibility of Fourier domain measurements in healthy subjects. *Methods*. One hundred and thirty-two eyes of 132 healthy subjects were scaned on the same day with both instruments, separated by 10 minutes from each other. Thickness of quadrant, average and the 12 different areas around the optic nerve were compared between Cirrus and Stratus. Repeatability, intraclass correlation coefficients (ICCs), and coefficients of variation (COVs) were calculated in RNFL measurements provided by Fourier domain device. *Results*. The average thickness in the optic cube was 95.50 μm using Cirrus and 97.85 μm using Stratus. Average thickness and temporal quadrant showed significant differences using Cirrus and Stratus methods. Reproducibility was better with Fourier domain OCT (mean COV of 4.54%) than with Stratus time-domain OCT (mean COV of 5.57%). *Conclusions*. Both scan options give reproducible RNFL thickness measurement, but there are differences between them. Measurements obtained using Fourier domain device show better reproducibility.

1. Introduction

Optic nerve diseases, including glaucoma and other neurological pathologies, need and objective, quantitative, and sensitive method to assess retinal nerve fiber layer (RNFL) thickness both for diagnosing and monitoring their progression. The importance of RNFL thickness determination in the early diagnosis of glaucoma cannot be overstated, because RNFL thinning may in theory be the earliest structural change clinically detectable and has been shown to precede functional loss by as much as 5 years [1]. RNFL thickness maps can also be potentially used for a thorough evaluation of the RNFL in the longitudinal monitoring optic nerve disease, which is extremely important in the clinical management of a life-long disease.

Optical coherence tomography (OCT) is nowadays an important diagnostic tool for retinal diseases in the clinical practice. It provides cross-sectional or three-dimensional images by measuring the echo time delay and magnitude of backscattered or back-reflected light. The OCT gives a kind of optical biopsy with quantitative and reproducible measurements of macular and RNFL thickness parameters using near-infrared light [2, 3]. OCT was first developed as a research tool in 1991 obtaining two-dimensional images [4, 5] using low-coherence interferometry to measure the time delay of back-scattered light from different layers of the retina. Time domain OCT (TDOCT) technology was the first introduced. The standard in OCT retinal imaging was the Stratus-OCT (Carl Zeiss Meditec Inc, Dublin, California, USA). Stratus OCT was widely used in clinical settings, and

provided detailed cross-sectional images and quantitative information of the retina with an axial resolution of 10 μm and a scan velocity of 400 axial scans per second [6, 7]. Stratus OCT has demonstrated its ability to detect RNFL loss [8]. For the past last years, improved OCT devices employing spectral domain OCT (SDOCT) or Fourier-domain OCT (FDOCT) have been introduced in the clinical practice. Fourier domain detection can measure all echoes of light from different delays simultaneously. This technology features greater scan acquisition speed, higher resolution images, and more reproducible measurements. The higher acquisition speed reduces the eye motion artefacts and enables a better delineation of the retinal layers [9]. It is then possible to detect and segment the retinal structures in each raster OCT image [10]. FDOCT provides a faster scanning of the tissue achieving an axial resolution up to five times higher and imaging speeds up to 60 times greater than conventional OCT [11–14]. Cirrus high definition (HD) OCT (Carl Zeiss Meditec) is a FDOCT that has an axial resolution of 5 μm and a scan velocity of 27,000 axial scans per second.

Several studies have reported the importance of RNFL thickness determination in the early diagnosis and managing of optic nerve conditions, such as glaucoma [15], band atrophy with or without chiasmal compression [16], demyelinating diseases [17, 18], and optic neuritis. This topic based on OCT can reveal changes in RNFL thickness before visual field defects appear [19]. It is important that these new techniques are capable of marking accurate, reliable, and reproducible measurements, because the results of the RNFL thickness evaluations may vary widely according to the devices used.

The repeatability and reliability of retinal thickness measurements using Stratus OCT has been probed in several studies [20, 21]. Different studies had also demonstrated that FDOCT are very reliable devices [18, 22, 23].

An essential quality in determining the utility of a device for clinical use is its measurement reproducibility. The goal of our present study was to compare the RNFL measurements in healthy persons using both OCT methods and to determine the reproducibility of RNFL measurements with both instruments.

2. Material and Methods

We carried out a prospective cross-sectional study including 132 consecutive healthy subjects who were imaging with Stratus OCT and Cirrus HD OCT on the same day. One randomly selected eye of each subject was analyzed. All the procedures were conducted in accordance with the principles of Helsinki Declaration and the experimental protocol was approved by the local Ethics Committee. Detailed consent forms were obtained from each subject.

For Cirrus HD and Stratus instruments the RNFL is presented on two circular charts, one with 12 equal sectors each representing one clock hour and the other with four equal 90° sectors, each representing one quadrant (temporal: 316–45°on unit circle, superior: 46–135°, nasal: 136–225° and inferior quadrant: 226–315°). The chart displays microns of the RNFL thickness. Average RNFL thickness (0°–359°) is also displayed.

All the subjects underwent a comprehensive ophthalmic examination including medical, ocular and family history, best corrected visual acuity (BCVA), visual field, slit lamp biomicroscopy, intraocular pressure (IOP) measurements with Goldmann applanation tonometry, and fundoscopy examination.

The included persons had BCVA of 20/25 or better according to the Snellen scale, a normal visual field (VF) examination, and no history of ocular or neurological disease. Exclusion criteria were the presence of significant refractive errors (more than 5 diopters of spherical *equivalent refraction* or 3 diopters of astigmatism), IOP of 21 mmHg or higher, media opacifications, systemic conditions that could affect the visual system, a history of ocular trauma or concomitant ocular diseases, including a previous history of retinal pathology, glaucoma, laser therapy, or ocular pathologies affecting the cornea, lens, retina, or optic nerve.

The VF was assessed using a Humphrey Field Analyzer (Carl-Zeiss Meditec, Dublin, CA). A SITA Standard strategy (program 30-2) was used to decrease the duration of the exam.

Each subject was imaged with the two OCTs on the same day without dilating the pupil. Fast RNFL thickness (3.46) and optic disc cube 200 × 200 were the scan acquisition protocols used for measuring the peripapillary RNFL thickness with the TDOCT and Fourier-domain FDOCT, respectively. This diameter was set by Schuman et al. because it is large enough to avoid the overlap with the optic nerve head in almost all the eyes and yet allow measurement in an area with thicker RNFL [2].

In order to study the reproducibility of the measurement, all the subjects underwent 3 different 3.4 mm diameter circular scans centered on the optic disc with the Cirrus HD OCT, with 10 minutes of time between each other. To have our own Stratus OCT reproducibility, 90 of the total subjects had three different scans following the same procedure. The two OCTs were used in random order to prevent any effect of fatigue bias.

Between scan acquisitions, there was a time delay and subject position and focus were randomly disrupted, meaning that alignment parameters had to be newly adjusted at the start of each image acquisition. No manual correction was applied to the OCT output. An internal fixation target was used because it has previously been shown to give the highest reproducibility [2].

Following the recommended procedure for scan acquisition, the subject's pupil was first centered and focused in an iris viewing camera on the system data acquisition screen, and then the system's line-scanning ophthalmoscope was used to optimize the view of the retina. The OCT scan was aligned to the proper depth and patient fixation, and system polarization was optimized to maximize the OCT signal.

Three repetitions of optic disc cube 200 × 200 scans in each eye were performed using both OCT devices. The Cirrus HD OCT optic disc protocol generates a map with average RNFL thickness, quadrant RNFL thickness (superior, nasal, inferior and temporal), and 12 clock hours of 30° RNFL

thickness. The numeration of the hour sectors was assigned from position H1 to H12 in the clockwise direction for the right eye and in the counterclockwise direction for the left eye. Same data are provided by Stratus OCT.

The presence of defects in the RNFL can be detected using both devices (Stratus and Cirrus HD OCT) and is provided by the comparison of measurements from each patient with the normative database of each instrument.

Two investigators (I. Pinilla, E. Garcia-Martin) judged the scans to be of acceptable quality and selected only the scans were optic disc was centered and focused within the circular scan, using fundus images captures on OCT scan printout. All the scans had continuous lines for demarcating the RNFL border. Only subjects with good images obtained with both OCTs were selected for the study. Cirrus HD and Stratus OCT determine the quality of images using the signal strength measurement that combines signal-to-noise ratio with the uniformity of the signal within a scan and is measured on a scale of 1 to 10, where 1 is categorized as poor image quality and 10 as excellent image quality. Only images with a score higher than 7 were evaluated in our study. Three series of good quality scans were obtained for each option. Twenty-nine images with artifacts, missing parts, or showing seemingly distorted anatomy were excluded [24]. To obtain good quality and centered images, ten eyes required repeat scan acquisition using the Cirrus HD OCT and twenty-three eyes using the Stratus OCT.

2.1. Statistical Analysis. Statistical software (SPSS 15.0, SPSS Inc., Chicago, IL) was used for statistical analysis. The Kolmogorov-Smirnov test was used to assess sample distribution. The Cirrus HD values were analyzed using the mean of the three measurements. The average RNFL thickness and the RNFL in each quadrant and in each 30° segment were tested for statically disparity between both OCT instruments. All the results were expressed as mean ± standard deviation (±SD).

Differences between Cirrus HD and Stratus RNFL measurements in each group were also compared using a Student's t-test for paired data. Values of $P < 0.05$ were considered to be indicative of statistically significant differences. Comparisons of RNFL thickness between the two instruments were graphically represented.

Variability was assessed by computing for each parameter the standard deviation of the mean, repeatability, coefficient of variance and intraclass correlation coefficient. For each parameter, the coefficient of variation (COV) was calculated as the standard deviation divided by the average of the measurement value and expressed as a percentage. Most authors consider that devices with a COV less than 10% have high reproducibility, while a COV less than 5% indicates very high reproducibility [22]. To assess the reliability of the repeated measurements, the intraclass correlation coefficients (ICCs) for absolute agreement were calculated. They measure the concordance for continuous variables and correct correlations for systematic bias. The ICC interpretation that we used was slight reliability (for values between 0 and 0.2), fair reliability (from 0.21 to 0.4), moderate reliability (values between 0.41 and 0.6), substantial reliability (values from 0.61 to 0.8), and almost perfect reliability (for values of intraclass correlation coefficients higher than 0.81). Bland and Altman plots were used to assess agreement. Reproducibility of both devices was also represented by displaying the differences between measurements by the two instruments against the mean of the two measurements (Bland-Altman plots) [25].

3. Results and Discussion

Table 1 gives the mean values and standard deviation of the RNFL in global thickness and in each parapapillary quadrant in all the subjects. Significant differences were found in the global thickness using both instruments; this value was 2.37 microns superior with Stratus than with Cirrus HD OCT ($P = 0.003$). Significant differences were only found between the temporal quadrants measurements with both instruments (2.21 μm higher using Stratus; $P = 0.046$). When the different 12 segments around the optic disc were analyzed, we found significant differences in sectors H1, H4, H5, H8, H11, and H12 (see Table 1). The quadrant thickness differences between both OCT devices are shown in Figure 1. The graph demonstrates that measurements of RNFL thickness were thicker with the Stratus OCT than with the Cirrus HD OCT. Also, the inspection of the plots reveals discrepancy between RNFL thickness measurements obtained by both OCT instruments.

Reproducibility is presented in Table 2. Bland-Altman plots were made depicting the agreement between different Cirrus HD OCT RNFL thickness measurements (Figure 2) and Stratus measurements (Figure 3). The difference between Cirrus HD OCT measurements (first Cirrus HD OCT RNFL thickness-second Cirrus HD OCT RNFL thickness) was plotted against the average of the three Cirrus HD OCT measurements for the RNFL thickness (Figure 2). The scatterplots demonstrate the agreement of the measurements. More than 90% of the measurements were between ±5 microns differences (Figures 2 and 3). These small differences were not related to the average RNFL thickness and were similar in those with thinner or smaller thickness. Variability of RNFL measurements was higher with Stratus OCT, as is shown in Tables 1 and 2, and Figure 3.

In most of the cases, direct comparison of RNFL measurements on the same eyes using both OCT instruments showed that the Stratus OCT gave a thinner measurement of the RNFL. As it would be expected, there was high correlation between measurements taken by both devices, and when differences between measurements were evaluated using Bland-Altman plots, considerable discrepancy between the two instruments was observed (Figure 4). Some authors have designed a correction factor to predict the RNFL measurement using other OCT devices, but this analysis is only an approximation.

As previous authors have described, regional reproducibility data shows the nasal quadrant to be the least reproducible (highest root mean squared error) (Table 2) [18, 22]. When incorporating the RNFL thickness into a reproducibility calculation, the coefficient of variation for

Table 1: Mean retinal nerve fiber layer parameters and standard deviation measured by Cirrus high definition (HD) and Stratus optical coherence tomography (OCT) and their statistical comparisons.

	Stratus OCT parameters		Cirrus HD OCT parameters		Mean difference (Stratus-Cirrus)	*P*
	Mean	SD	Mean	SD		
Average thickness	97.85	11.47	95.50	9.45	2.37	***0.003***
Superior thickness	119.54	19.47	117.06	17.32	2.63	0.070
Nasal thickness	74.44	19.83	71.41	16.55	2.96	0.106
Inferior thickness	126.38	18.87	125.36	16.63	1.09	0.357
Temporal thickness	70.99	13.62	68.38	11.81	2.21	***0.046***
H1 hour sector	110.65	29.35	103.77	26.41	7.17	***0.004***
H2 hour sector	90.02	26.71	87.49	19.34	2.36	0.317
H3 hour sector	59.84	17.15	56.86	11.99	2.91	0.068
H4 hour sector	73.01	20.62	66.23	16.13	6.83	***0.000***
H5 hour sector	106.28	26.12	101.65	24.34	4.79	***0.006***
H6 hour sector	134.54	27.42	133.72	29.47	0.86	0.657
H7 hour sector	141.86	26.31	138.64	24.48	2.52	0.203
H8 hour sector	75.32	18.56	71.88	18.35	4.17	***0.006***
H9 hour sector	53.40	10.61	53.87	13.77	-0.05	0.968
H10 hour sector	82.24	19.83	82.92	20.52	-0.79	0.620
H11 hour sector	131.51	24.56	126.84	25.65	4.75	***0.023***
H12 hour sector	123.05	25.81	115.65	26.25	7.63	***<0.001***

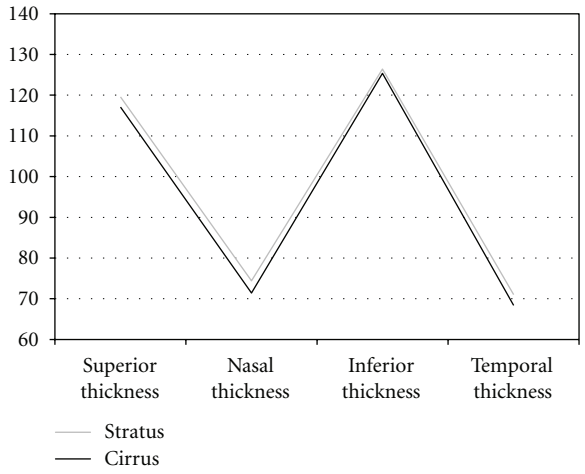

Figure 1: Representation for retinal nerve fiber layer thicknesses in the four quadrants using Cirrus HD and Stratus OCT devices. Measurements were higher with Cirrus OCT.

Table 2: Coefficients of variation (COVs) and intraclass coefficients (ICCs) for repeated retinal nerve fiber layer thickness measurements using Cirrus HD and Stratus optical coherence tomography.

	Cirrus HD OCT		Stratus OCT	
	COV	ICC	COV	ICC
Average thickness	1.64	0.985	2.22	0.978
Superior quadrant	3.37	0.970	4.46	0.899
Nasal quadrant	4.80	0.886	4.03	0.950
Inferior quadrant	3.57	0.943	5.78	0.878
Temporal quadrant	3.51	0.956	5.99	0.780
H1	5.30	0.972	6.76	0.956
H2	5.58	0.954	6.08	0.905
H3	4.49	0.957	5.40	0.923
H4	5.33	0.963	5.87	0.938
H5	5.39	0.964	5.94	0.897
H6	5.62	0.947	6.98	0.905
H7	4.24	0.964	5.48	0.938
H8	5.61	0.944	6.91	0.923
H9	3.98	0.931	5.75	0.919
H10	3.80	0.977	4.53	0.969
H11	4.59	0.934	4.96	0.866
H12	6.37	0.936	7.70	0.845

* COVs, coefficients of variation (in %); ICCs, intraclass coefficients.

the superior and inferior quadrants is smaller than for the nasal and temporal quadrants. This is due to the smaller mean RNFL thickness values in the nasal and temporal quadrants. Gürses-Ozden et al. demonstrated that increasing the number of A scans per acquisition fourfold significantly reduced the coefficient of variation in those quadrants with corresponding visual field defects [26].

RNFL measurements obtained in this reproducibility study are consistent with known properties of the RNFL with thicker superior and inferior nerve fiber bundles in normal eyes. There are many potential explanations for variability in RNFL measurements. Factors such as media opacity, pupil dilatation sampling density, type of scan, and the quadrant measured may all have effects on the overall scan quality and the calculated RNFL thickness [15, 27, 28]. The variability of measurements attributable to different operators and different sessions within the same visit has been shown to be relatively small [28]. In summary, our results indicate that

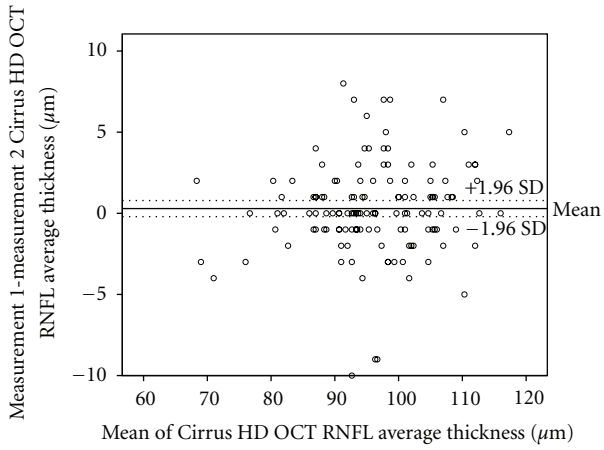

Figure 2: Bland-Altman plots of the agreement in retinal nerve fiber layer (RNFL) thickness between Cirrus HD OCT measurement 1 and Cirrus HD OCT measurement 2. The difference (Cirrus HD OCT average RNFL thickness measurement 1 minus Cirrus HD OCT average RNFL thickness measurement 2) was plotted against the average of the three measurements for the average RNFL thickness Cirrus HD OCT measurements. SD: standard deviation.

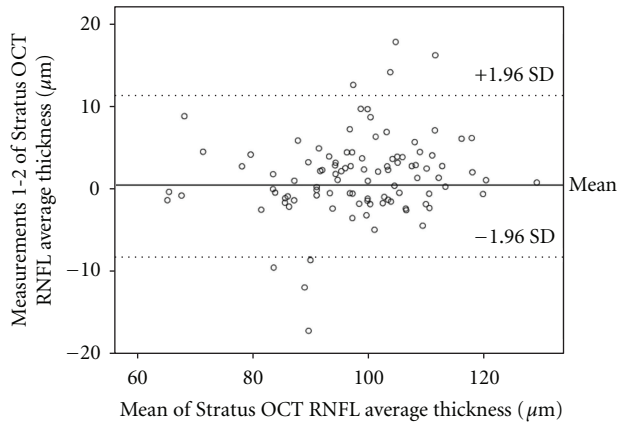

Figure 3: Bland-Altman plots of the agreement in retinal nerve fiber layer (RNFL) thickness between Stratus OCT measurement 1 and measurement 2. The difference (Stratus OCT average RNFL thickness measurement 1 minus Stratus OCT average RNFL thickness measurement 2) was plotted against the average of the three measurements for the average RNFL thickness Stratus OCT measurements. SD: standard deviation.

the reproducibility of OCT is adequate for assessing long-term followup for any optic neuropathy or RNFL damage.

4. Conclusions

Stratus and Cirrus high definition optical coherence tomography devices give good retinal nerve fiber layer thickness measurements with differences between their values. The reproducibility of RNFL measurements using Stratus time domain OCT is good and excellent with Cirrus HD Fourier domain OCT.

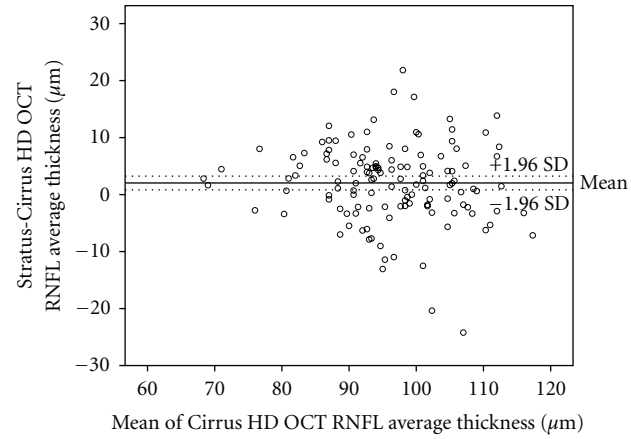

Figure 4: Bland-Altman plots of the agreement in retinal nerve fiber layer (RNFL) thickness between Stratus OCT and Cirrus HD OCT. The difference (Stratus OCT average RNFL thickness minus Cirrus HD OCT average RNFL thickness) was plotted against the average of the three measurements for the average RNFL thickness Cirrus HD OCT measurements. SD: standard deviation.

Conflict of Interests

The authors have no proprietary interests. No conflicting relationship exists for any author.

Acknowledgments

The authors acknowledge receiving Spanish Grant from the Carlos III Institute (FIS PI11/01553, PS09/1854) Grupo de Investigación en Retina (RD07-0062) and DGA/IIS Aragón. The authors would like to thank Dr. Antonio Ferreras and Prof. Luis E. Pablo for their technical support.

References

[1] A. Sommer, J. Katz, H. A. Quigley et al., "Clinically detectable nerve fiber atrophy precedes the onset of glaucomatous field loss," *Archives of Ophthalmology*, vol. 109, no. 1, pp. 77–83, 1991.

[2] J. S. Schuman, T. Pedut-Kloizman, E. Hertzmark et al., "Reproducibility of nerve fiber layer thickness measurements using optical coherence tomography," *Ophthalmology*, vol. 103, no. 11, pp. 1889–1898, 1996.

[3] E. Z. Blumenthal, J. M. Williams, R. N. Weinreb, C. A. Girkin, C. C. Berry, and L. M. Zangwill, "Reproducibility of nerve fiber layer thickness measurements by use of optical coherence tomography," *Ophthalmology*, vol. 107, no. 12, pp. 2278–2282, 2000.

[4] D. Huang, E. A. Swanson, C. P. Lin et al., "Optical coherence tomography," *Science*, vol. 254, no. 5035, pp. 1178–1181, 1991.

[5] J. M. Bland and D. G. Altman, "Statistical methods for assessing agreement between two methods of clinical measurement," *The Lancet*, vol. 1, no. 8476, pp. 307–310, 1986.

[6] J. G. Fujimoto, D. Huang, M. R. Hee et al., "Physical properties of optical coherence tomography," in *Optical Coherence Tomography of Ocular Diseases*, J. S. Schuman, C. A. Pulido, and J. G. Fujimoto, Eds., pp. 677–688, SLACK Incorporated, Thorofare, NJ, USA, 2nd edition, 2004.

[7] D. Huang, T. Ou, J. Fujimoto et al., "Optical coherence tomography," in *Retinal Imaging*, D. Huang, P. K. Kaiser, C. Y. Lowder, and E. I. Traboulsi, Eds., pp. 47–65, Mosby Elsevier, Philadelphia, Pa, USA, 2006.

[8] M. L. R. Monteiro, B. C. Leal, F. C. Moura, R. M. Vessani, and F. A. Medeiros, "Comparison of retinal nerve fibre layer measurements using optical coherence tomography versions 1 and 3 in eyes with band atrophy of the optic nerve and normal controls," *Eye*, vol. 21, no. 1, pp. 16–22, 2007.

[9] W. Drexler and J. G. Fujimoto, "State-of-the-art retinal optical coherence tomography," *Progress in Retinal and Eye Research*, vol. 27, no. 1, pp. 45–88, 2008.

[10] M. L. Gabriele, H. Ishikawa, G. Wollstein et al., "Peripapillary nerve fiber layer thickness profile determined with high speed, ultrahigh resolution optical coherence tomography high-density scanning," *Investigative Ophthalmology and Visual Science*, vol. 48, no. 7, pp. 3154–3160, 2007.

[11] M. Wojtkowski, V. J. Srinivasan, T. H. Ko, J. G. Fujimoto, A. Kowalczyk, and J. S. Duker, "Ultrahigh-resolution, high-speed, Fourier domain optical coherence tomography and methods for dispersion compensation," *Optics Express*, vol. 12, no. 11, pp. 2404–2422, 2004.

[12] M. Wojtkowski, V. Srinivasan, J. G. Fujimoto et al., "Three-dimensional retinal imaging with high-speed ultrahigh-resolution optical coherence tomography," *Ophthalmology*, vol. 112, no. 10, pp. 1734–1746, 2005.

[13] M. Wojtkowski, V. Srinivasan, T. Ko et al., "High speed, ultrahigh resolution retinal imaging using spectral/fourier domain OCT," in *2005 Conference on Lasers and Electro-Optics, CLEO*, pp. 2058–2060, usa, May 2005.

[14] M. A. Choma, M. V. Sarunic, C. Yang, and J. A. Izatt, "Sensitivity advantage of swept source and Fourier domain optical coherence tomography," *Optics Express*, vol. 11, no. 18, pp. 2183–2189, 2003.

[15] D. L. Budenz, S. T. Chang, X. Huang et al., "Reproducibility of retinal nerve fibre layer measurements using the Stratus OCT in normal and glaucomatous eyes," *Investigative Ophthalmology & Visual Science*, vol. 46, no. 7, pp. 2440–2446, 2005.

[16] L. V. F. Costa-Cunha, L. P. Cunha, R. F. S. Malta, and M. L. R. Monteiro, "Comparison of Fourier-domain and time-domain optical coherence tomography in the detection of band atrophy of the optic nerve," *American Journal of Ophthalmology*, vol. 147, no. 1, pp. 56–e2, 2009.

[17] E. Gordon-Lipkin, B. Chodkowski, D. S. Reich et al., "Retinal nerve fiber layer is associated with brain atrophy in multiple sclerosis," *Neurology*, vol. 69, no. 16, pp. 1603–1609, 2007.

[18] E. Garcia-Martin, V. Pueyo, I. Pinilla, J. R. Ara, J. Martin, and J. Fernandez, "Fourier-domain OCT in multiple sclerosis patients: reproducibility and ability to detect retinal nerve fiber layer atrophy," *Investigative Ophthalmology & Visual Science*, vol. 52, no. 7, pp. 4124–4131, 2011.

[19] J. Gyatsho, S. Kaushik, A. Gupta, S. S. Pandav, and J. Ram, "Retinal nerve fiber layer thickness in normal, ocular hypertensive, and glaucomatous Indian eyes: an optical coherence tomography study," *Journal of Glaucoma*, vol. 17, no. 2, pp. 122–127, 2008.

[20] V. Gupta, P. Gupta, R. Singh, M. R. Dogra, and A. Gupta, "Spectral-domain cirrus high-definition optical coherence tomography is better than time-domain stratus optical coherence tomography for evaluation of macular pathologic features in uveitis," *American Journal of Ophthalmology*, vol. 145, no. 6, pp. 1018–e2, 2008.

[21] V. Pierre-Kahn, R. Tadayoni, B. Haouchine, P. Massin, and A. Gaudric, "Comparison of optical coherence tomography models OCT1 and Stratus OCT for macular retinal thickness measurement," *British Journal of Ophthalmology*, vol. 89, no. 12, pp. 1581–1585, 2005.

[22] E. Garcia-Martin, I. Pinilla, M. Idoipe, I. Fuertes, and V. Pueyo, "Intra and interoperator reproducibility of retinal nerve fibre and macular thickness measurements using Cirrus Fourier-domain OCT," *Acta Ophthalmologica*, vol. 89, no. 1, pp. e23–e29, 2011.

[23] E. Garcia-Martin, I. Pinilla, E. Sancho et al., "OCT in retinitis pigmentosa: reproducibilityand capacity to detect macular and retinal nerve fiber layer thickness alterations," *Retina*. In press.

[24] Z. Wu, J. Huang, L. Dustin, and S. R. Sadda, "Signal strength is an important determinant of accuracy of nerve fiber layer thickness measurement by optical coherence tomography," *Journal of Glaucoma*, vol. 18, no. 3, pp. 213–216, 2009.

[25] J. M. Bland and D. G. Altman, "Statistical methods for assessing agreement between two methods of clinical measurement," *The Lancet*, vol. 1, no. 8476, pp. 307–310, 1986.

[26] R. Gürses-Ozden, C. Teng, R. Vessani, S. Zafar, J. M. Liebmann, and R. Ritch, "Macular and retinal nerve fiber layer thickness measurement reproducibility using optical coherence tomography (OCT-3)," *Journal of Glaucoma*, vol. 13, no. 3, pp. 238–244, 2004.

[27] L. A. Paunescu, J. S. Schuman, L. L. Price et al., "Reproducibility of nerve fiber thickness, macular thickness, and optic nerve head measurements using StratusOCT," *Investigative Ophthalmology and Visual Science*, vol. 45, no. 6, pp. 1716–1724, 2004.

[28] E. Z. Blumenthal and R. N. Weinreb, "Assessment of the retinal nerve fiber layer in clinical trials of glaucoma neuroprotection," *Survey of Ophthalmology*, vol. 45, supplement 3, pp. S305–S312, 2001.

Hindawi Publishing Corporation
Journal of Ophthalmology
Volume 2012, Article ID 564627, 7 pages
doi:10.1155/2012/564627

Clinical Study

Time-Domain and Spectral-Domain Optical Coherence Tomography of Retinal Nerve Fiber Layer in MS Patients and Healthy Controls

Alex P. Lange,[1] Reza Sadjadi,[2] Jameelah Saeedi,[2] Janette Lindley,[1] Fiona Costello,[3] and Anthony L. Traboulsee[2]

[1] *Neuro-Ophthalmology Division, Department of Ophthalmology, Eye Care Center (VGH), The University of British Columbia, 2550 Willow Street, Vancouver, BC, Canada V5Z 3N9*
[2] *Division of Neurology, Department of Medicine, University of British Columbia, S199 Koerner Pavillion, Wesbrook Mall, Vancouver, BC, Canada V6T 2B5*
[3] *Departments of Clinical Neurosciences and Surgery and Hotchkiss Brain Institute, University of Calgary, Calgary, AB, Canada T2N 1N4*

Correspondence should be addressed to Alex P. Lange, alex@lange.ch

Received 22 January 2012; Accepted 14 March 2012

Academic Editor: Robert J. Zawadzki

Objective. The aim of this study was to compare retinal nerve fiber layer thickness (RNFLT) between spectral-domain (SD-) and time-domain optical coherence tomography (TD-OCT) in MS patients and healthy controls (HC). Furthermore, RNFLT between MS eyes with and without optic neuritis (ON) and HC should be explored. Finally, the relationship between RNFLT, disease duration, EDSS, and disease modifying therapy (DMT) should be established. *Design*. Prospective, cross-sectional study. *Participants*. 28 MS patients and 35 HC. *Methods*. Both groups underwent TD- and SD-OCT measurements. RFNLT was correlated between the two machines and between MS eyes with and without ON and HC. Furthermore, RNFLT was correlated to disease duration, EDSS and DMT. *Results*. A strong correlation (Pearson's $r = 0.921$, $P < 0.001$), but a statistically significant difference of 2 μm ($P < 0.001$), was found between the two devices. RNFLT was significantly different between MS eyes with history of ON (mean RFNLT (SD) 72.21 μm (15.83 μm)), MS eyes without history of ON 93.03 μm (14.25 μm), and HC 99.07 μm (7.23 μm) ($P < 0.001$). *Conclusions*. The measurements between different generation of OCT machines are not interchangeable, which should be taken into account if comparing results between different machines and switching OCT machine in longitudinal studies.

1. Introduction

Optical coherence tomography (OCT) is a noninvasive technique for high-resolution, cross-sectional tomographic imaging of retinal tissue using backscattered light. OCT imaging is very similar to ultrasound B-Scan imaging but uses infrared-light instead of ultrasound waves. Two-dimensional, cross-sectional images are obtained from multiple axial scans (A-Scans) at different transverse locations [1].

Until recently, third-generation time-domain OCT (TD-OCT) using Stratus OCT (Carl Zeiss Meditec AG, Jena, Germany) has been widely used to acquire images at a rate of 400 axial scans per second with an axial resolution of 10 μm [2]. The recently introduced fourth-generation spectral-domain OCT (SD-OCT) has improved depth resolution by a factor of three (axial resolution up to 3.8 μm) and allows a significantly higher acquisition speed (40'000 axial scans per second) resulting in improved image quality and minimized motion artefacts [3]. Furthermore, software improvements allow reconstruction of a three-dimensional image of the retina.

Heidelberg Spectralis OCT (Heidelberg Engineering, Heidelberg, Germany) uses an integrated eye tracking system (IETS) to compensate for eye movement artefact during data acquisition. IETS also allows an automatic re-centration, which can be used for more reliable follow-up scans.

Heidelberg noise reduction technology helps producing significantly improved images by adjusting data and reducing noise using mean values from several scans [4]. Heidelberg Spectralis OCT needs to be validated for accuracy, reproducibility, and comparability to previous models before it can be reliably used for clinical and research purposes.

Recent studies have shown differences between SD-OCT machines (Cirrus SD-OCT, Carl Zeiss Meditec AG, Jena, Germany [5–10], RTVue-100, Optovue Inc., Fremont, CA, USA [11], and Spectralis, Heidelberg Engineering, Heidelberg, Germany, [12, 13]) and TD-OCT in healthy controls and glaucoma patients. These studies showed better reproducibility compared to TD-OCT and significant differences in RNFLT measurements between the two generations of machines.

So far only few studies have examined the role of SD-OCT in multiple sclerosis (MS) patients [14, 15]. Therefore, our specific study aims are (1) to compare retinal nerve fiber layer thickness (RNFLT) measurements between the validated third-generation Stratus OCT and the new fourth-generation Heidelberg Spectralis OCT in MS patients and healthy controls, (2) to compare RNFLT between MS eyes affected by optic neuritis (ON eyes) to eyes without a history of ON (NON eyes) and control eyes, and finally (3) to determine the relationship between RNFLT, disease duration, expanded disability status scale (EDSS), and disease-modifying therapy (DMT) in MS patients and refraction in both groups.

2. Materials and Methods

2.1. Study Design and Patient Population. In a prospective, cross-sectional study, subjects with MS and controls were identified from the UBC Hospital MS Clinic with the aid of advertisement and pamphlets. All MS subjects had confirmed diagnosis of MS made by a neurologist with specific experience in managing MS patients, and based on the modified McDonald criteria [16].

2.2. Inclusion and Exclusion Criteria. Patients with a recent history of optic neuritis (ON) (<6 months), history of ocular diseases (age-related macular degeneration, diabetic retinopathy, uveitis, and glaucoma), and history of other diseases that could mimic MS or affect OCT testing (neuromyelitis optica, parkinson's disease, and Alzheimer disease) and subjects with difficulties maintaining fixation were not included.

2.3. Outcome Measures

2.3.1. Clinical Data. Clinical history information such as disease duration from time of disease onset, previous history of optic neuritis, and other neurological information like EDSS score was obtained by history and from hospital charts after patient recruitment. Myopia was defined as spherical equivalent of <-0.50 diopters, emmetropia between -0.5 and $+0.5$ diopters, and hyperopia as $>+0.5$ diopters measured by SD-OCT.

Table 1: Descriptive statistics of MS and control group.

	Control group	MS group
N	35	28
Mean age in years (±SD)	38.88 (11.65)	43.46 (9.08)
Gender	15 female 20 male	23 female 5 male
Number excluded	2	1
Average RNFL SD-OCT (micrometer ± SD)	98.59 (6.74)	88.80 (17.39)
Average RNFL TD-OCT (micrometer ± SD)	100.67 (8.88)	90.91 (18.09)
Number of eyes with optic neuritis	n/a	14 (26%)
Number of patients with SPMS	n/a	3 (11%)
Mean EDSS (SD)	n/a	2.8 (1.6)
Mean disease duration in months (SD)	n/a	83.12 (83.67)
On disease-modifying therapy	n/a	52% (14/27)

2.3.2. Optical Coherence Tomography. OCT was performed in a random order by an experienced person that was masked to clinical data, using TD-OCT and SD-OCT within one-hour period with no pupil dilation (half of subjects had TD-OCT prior to SD-OCT and vice versa).

TD-OCT (Stratus OCT 3000, Software Version 4.0.7; Carl Zeiss Meditec, Jena, Germany): the standard Fast RNFL acquisition protocol was used. Three scans, each composed of 256 A scans, were automatically acquired consecutively using a circle scan with a standardized diameter of 3.4 mm by the same experienced operator. Several scans were taken and the best-centered scan with a quality score of ≥ 6 was chosen for analysis (as suggested by the manufacturer). An automated computer algorithm delineated the anterior and posterior margins of the RNFL.

SD-OCT (Heidelberg Spectralis OCT, Software Version 5.1.2, Heidelberg Engineering, Heidelberg, Germany): The RNFL protocol in high-resolution mode (axial resolution 3.8 μm, 19'000 scans per second) was used. Sixteen consecutive circular B-scans (each composed of 1536 A scans) with a diameter of 3.4 mm were automatically averaged to reduce speckle noise. The online tracking system compensated for eye movements. Several scans were taken by the same experienced operator and the best centered with a quality of at least 24 (which is about the equivalent of 6 in Stratus OCT) was chosen for analysis. The included software algorithm delineated the anterior and posterior margins of the RNFL.

2.4. Statistical Analysis. Microsoft Office 2007 and SPSS Version 16.0 for Windows were used to do statistical analysis. Descriptive, mean comparison (t-test and one-way ANOVA) and correlation analysis (Pearson's) were used to compare OCT measures between different groups: SD-OCT versus TD-OCT RNFLT measurements; MS eyes versus control eyes; myopic versus emmetropic and hyperopic eyes. P values less than 0.05 were considered to be statistically significant.

Table 2: Differences in RNFLT between SD- and TD-OCT in MS group and control group (SD-OCT minus TD-OCT).

	Control group		MS group	
	Mean difference in μm (95% CI)	Pearson's Corr r	Mean difference in μm (95% CI)	Pearson's Corr r
Average	−2.40 (−3.70 to −1.09)	0.83 ($P < 0.001$)	−1.69 (−3.44 to 0.06)	0.93 ($P < 0.001$)
Superior	3.75 (0.99 to 6.51)	0.77 ($P < 0.001$)	5.54 (2.20 to 8.87)	0.90 ($P < 0.001$)
Temporal	0.04 (−1.41 to 1.50)	0.88 ($P < 0.001$)	−0.54 (−3.02 to 1.94)	0.87 ($P < 0.001$)
Inferior	−6.56 (−8.28 to −4.84)	0.85 ($P < 0.001$)	−6.81 (−9.51 to −4.11)	0.91 ($P < 0.001$)
Nasal	−6.93 (−9.47 to −4.38)	0.80 ($P < 0.001$)	−3.37 (−7.13 to 0.40)	0.81 ($P < 0.001$)

3. Results

3.1. Patient Demographics and Clinical Characteristics. The study recruitment took place between August 2009 and February 2010. Twenty-eight MS patients (age mean: 38.88 yrs; SD: 11.65 yrs, mean disease duration: 83.12 months, SD: 83.76; 25 with relapsing-remitting and 3 with secondary progressive MS; EDSS range between 1.5 and 6.5, mean: 2.8, SD: 1.6) and 35 healthy controls (age mean: 43.46 yrs; SD: 9.08 yrs) participated in this study (Table 1). Fourteen (out of 27) patients used DMT for MS. Sixteen (out of 27) patients had an EDSS score of less than 3.0. All subjects were examined by SD-OCT and TD-OCT machines. Two subjects were excluded in the control group due to (1) software failure to delineate RNFL correctly and (2) OCT artefacts due to high myopia. One patient in the MS group was excluded due to inability to measure exact refraction after refractive surgery. Out of the remaining 120 eyes 32 eyes were myopic (refraction range between −8.25 and −0.75 diopters), 74 eyes were emmetropic (refraction = 0 diopters), and 14 eyes were hyperopic (refraction range between +1 and +6 diopters). Fourteen (out of 54) MS eyes were previously affected by a single optic neuritis event.

3.2. Comparing Time-Domain and Spectral-Domain OCT. SD-OCT and TD-OCT RNFLT values were strongly correlated in all quadrants with correlation coefficient ranging from 0.808 ($P < 0.01$) in inferior quadrant to 0.878 ($P < 0.01$) in temporal quadrant. The overall RNFLT was also strongly correlated (correlation coefficient = 0.921; $P < 0.001$) between the two machines (Figure 1). However, RNFLT values showed minor but statistically significant differences between the two machines ($P < 0.001$) (Table 2).

3.3. Comparing RNFLT Measurements between MS and Control Eyes. Overall, MS patients had significantly lower RNFLT measured by both SD-OCT and TD-OCT (Table 3). Moreover, RNFLT was significantly different between MS eyes with history of optic neuritis (mean RFNL (SD) 72.21 μm (15.83 μm)), MS eyes without history of optic neuritis 93.03 μm (14.25 μm), and healthy controls 99.07 μm (7.23 μm) ($P < 0.001$) measured by SD-OCT (Figure 2).

3.4. Correlation between Retinal Nerve Fiber Layer Thickness, Disease Duration, EDSS, DMT, and Refraction. When all MS eyes were considered, duration of the disease since onset of first symptoms weakly correlated with superior ($r = -0.28$; $P = 0.048$) and temporal ($r = -0.33$; $P = 0.02$) quadrant RNFLT. There was no significant correlation between disease duration and mean RNFLT values ($r = -0.13$; $P = 0.35$), or RNFLT values in the inferior ($r = -0.14$; $P = 0.31$) or nasal ($r = -0.19$; $P = 0.17$) quadrants. When only MS eyes without a history of ON were considered, a moderate correlation ($r = -0.44$; $P = 0.01$) was found between mean RNFLT and disease duration, with a significant correlation in the superior and inferior quadrants ($r = -0.51$; $P = 0.001$, and $r = -0.38$; $P = 0.02$, resp.) and no significant correlation in the temporal and nasal quadrants ($P = 0.91$ and $P = 0.08$, resp.).

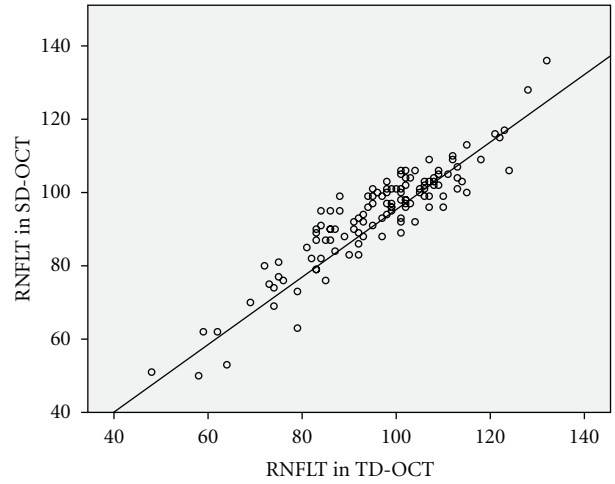

Figure 1: Correlation between average RNFLT in μm in SD-OCT (y-axis) and TD-OCT (x-axis).

When EDSS was correlated to mean RNFLT in all MS eyes, a weak correlation was found ($r = -0.3$; $P = 0.05$). This was significant in the superior quadrant only ($r = -0.33$; $P = 0.02$), nonsignificant in the other quadrants ($P = 0.46$ for temporal quadrant, $P = 0.07$ for inferior quadrant, and $P = 0.39$ for nasal quadrant). When only MS eyes without a history of ON were considered, a moderate correlation was found between EDSS and mean RNFLT ($r = -0.35$; $P = 0.03$). This was also significant in the superior ($r = -0.38$; $P = 0.02$) and inferior quadrants ($r = -0.33$; $P = 0.05$), but not in the temporal ($P = 0.31$) and nasal quadrants ($P = 0.43$).

Table 3: Overview RNFLT between SD- and TD-OCT in MS and control groups, separated by quadrants.

	SD-OCT μm mean (SD)		TD-OCT μm mean (SD)	
	Control	MS	Control	MS
Average	98.59 (6.79)	88.80 (17.55)	100.67 (8.96)	90.9107 (18.26)
Superior	121.27 (16.22)	107.25 (26.95)	117.48 (16.87)	101.88 (27.04)
Temporal	71.17 (10.88)	65.02 (15.92)	70.86 (12.88)*	65.82 (17.57)*
Inferior	127.16 (13.10)	114.80 (21.64)	133.23 (13.59)	120.36 (27.08)
Nasal	74.55 (11.21)	68.07 (21.53)	81.031 (15.75)	72.20 (24.34)

* All measures are significantly different between MS patients and control except for temporal quadrant measured by TD-OCT.

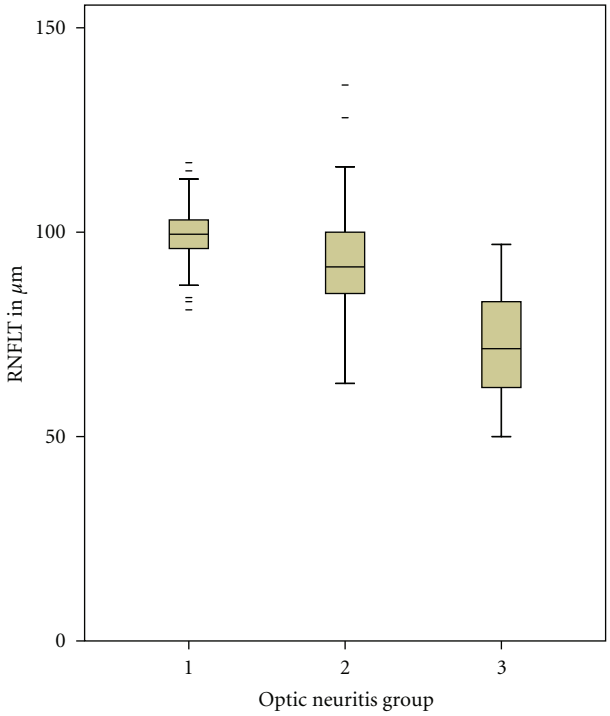

Figure 2: Boxplot of differences between RNFLT in control group (left box, group 1) and groups of MS eyes without optic neuritis (center box, group 2) and MS eyes with optic neuritis (left box, group 2) measured by SD-OCT.

The minimal difference between RFNLT in patients with DMT (86.07 μm) and without DMT (90.82 μm) was not statistically different ($P = 0.327$).

Myopic and emmetropic eyes showed significantly different RFNLT measurements in both SD-OCT (mean RNFLT (SD) 87.75 μm (12.52 μm) versus 96.46 μm (14.61 μm)) and TD-OCT (89.59 μm (13.65 μm) versus 99.19 μm (15.11 μm)). There was a significant correlation between refraction in diopters and RNFLT ($r = 0.4$; $P = 0.005$).

4. Discussion

The main aim of this study was to compare RNFLT measurements between SD-OCT and TD-OCT in MS patients and healthy controls. Our results show strong correlations (Pearson's $r = 0.921$) between the measurements of the Heidelberg Spectralis SD-OCT and TD-OCT. RNFLT values were significantly lower in SD-OCT (mean difference 2 μm). These results are similar to those of Watson et al. [14], who found Spectralis SD-OCT to measure 3 μm lower than TD-OCT in a study of 50 MS eyes, and Seibold et al. [12], who found the same results in a series of 80 healthy eyes. On the other hand, Arthur et al. [13] compared Spectralis SD-OCT with TD-OCT in 30 healthy eyes and found Spectralis to measure 6 μm lower, a larger difference than our results. Studies using other SD-OCT devices showed similar discrepancies with Cirrus SD-OCT measuring lower RNFLT and RTVue measuring higher RNFLT than TD-OCT (Table 4).

The discrepancy between different devices may be explained by a difference in calibration due to a higher resolution and improved software algorithm in more recent models [6]. This has been addressed in evaluation of SD-OCT in macular thickness [17, 18]. The phenomenon of thickness-dependent interdevice differences was not observed in our data [15]. The minimal difference observed in our study is lower than the axial resolution of the SD-OCT, hence clinically not significant. However, results from these machines cannot be interchangeably interpreted in a population study and ongoing longitudinal studies switching generation of OCT should take these differences into consideration.

There has been increasing interest in RNFLT measurements in MS patients in order to determine whether OCT can be used as a surrogate marker for follow-up examinations. Therefore, a large amount of cross-sectional data has been previously published. Many studies have shown differences between RNFLT in MS eyes with optic neuritis, MS eyes without optic neuritis, and healthy controls, for example, [15, 19–27]. All these studies were using the older TD-OCT technology. We were able to reproduce these differences using the newer generation of OCT machine. Spectral-domain OCT has several advantages over the older TD-OCT technology: there is no pupil dilation needed, the speed of the machines is higher, reducing the possibilities of motion artefacts, and the lack of the previously used bright flashlight makes the examination much more comfortable for the patient. Furthermore, the higher resolution and the improved software algorithm allowing automatic re-centration for follow-up exams help in improving accuracy

Table 4: Overview published studies comparing RNFLT in SD-OCT versus TD-OCT.

Author	SD-OCT used	Study population (eyes)	Results
Chang et al. [5]	Cirrus	54 glaucoma 50 controls	Cirrus is equivalent to Stratus for detecting glaucoma
Knight et al. [6]	Cirrus	101 glaucoma 29 controls	Cirrus 7 μm lower then Stratus in both groups
Leung et al. [7]	Cirrus	83 glaucoma 97 controls	Cirrus 12 μm lower for control, 6 μm lower in glaucoma
Sung et al. [8]	Cirrus	103 glaucoma 60 controls	Cirrus 13 μm lower for control, 14 μm lower in glaucoma
Vizzeri et al. [9]	Cirrus	78 glaucoma 32 controls	Cirrus 8 μm lower for control, 6 μm lower in glaucoma
Kim et al. [10]	Cirrus	27 controls	Cirrus 10 μm lower
Gonzalez-Garcia et al. [11]	RTVue-100	76 glaucoma 60 controls	RTVue 2 μm higher
Seibold et al. [12]	Cirrus, Spectralis, RTVue-100	80 controls	Spectralis 3 μm lower, Cirrus 12 μm lower, RTVue 3 μm higher,
Arthur et al. [13]	Spectralis	30 controls	Spectralis 6 μm lower
Watson et al. [14]	3D OCT-1000, Cirrus, RTVue-100, Spectralis	50 MS	Spectralis 3 μm lower, Cirrus 8 μm lower, RTVue 3 μm higher, 3D OCT-1000 2 μm higher
Bock et al. [15]	Cirrus	110 MS	Cirrus 8 μm lower

and reproducibility for follow-up exam in longitudinal studies. Up to date, no longitudinal study in an MS cohort has been published using SD-OCT technology. Two longitudinal studies using TD-OCT have not been able to show any change in RNFLT in a two-year follow-up period [27, 28]. Only Talman et al. [21] could detect significant RNFLT changes in a 4.5-year study of 299 patients using TD-OCT (loss of 2.9 μm at 2 to 3 years and 6.1 μm at 3 to 4.5 years; $P < 0.001$). This pattern was observed in both eyes with and without history of ON. Proportions of eyes with RNFL loss greater than test-retest variability ($\geq$6.6 μm) increased from 11% at baseline to 44% at final visit (3–4.5 years) ($P < 0.001$). The progressive axonal loss of approximately 2 μm per year could only be detected over a relatively long period of time. This is most likely due to the relatively low resolution of the TD-OCT machine. The new generation SD-OCT is more sensitive to smaller changes and may be more reliable detecting RNFL changes over shorter time periods. Longitudinal studies using SD-OCT technology will be needed to establish if OCT measurements can be used as a surrogate marker in MS and be used to monitor disease progression and disease-modifying therapy.

We were interested in contribution of disease duration, EDSS, refraction, and status of DMT on RNFLT measurements. Our results showed no significant correlation for disease duration and EDSS when all MS eyes were compared but moderate correlation when only eyes without a history of ON were considered. This may be due to the fact that ON causes a 18–22% loss of RNFLT and the small progressive loss of RNFLT is not evident at this time anymore [29]. The difference between patients with and without DMT was statistically not significant, but our sample size was too small for a final conclusion.

We also compared RNFLT measurements between refraction range groups (described in methods). We showed a relatively large difference between myopic and nonmyopic eyes using both devices. Thinner RNFLT measurements in myopes may be explained by increased scan diameter due to the telecentric optics of the OCT in increased myopia and myopic tilted discs resulting in elevated and decreased RNFLT at different sites. Furthermore, the centration is very difficult even on a frozen fundus image due to the asymmetry of the disc.

RNFLT values were significantly lower in myopic eyes as the diameter of the scan increases with higher myopic refraction. Rauscher et al. [30] have reported an average decrease of RNFL of 3 μm per diopter of myopia. A possible explanation is the telecentric system, which keeps the angle of the OCT beam constant at 12 degrees. In our measurements, the scan diameter increased to 3.8 mm in -5 diopters and to 4.2 mm in -10 diopters. This results in thinning of about 10 μm in -5 diopters and about 20 μm in -10 diopters [31]. This was not a major issue with the older TD-OCT as the axial resolution is only 10 μm but gets more importance with the SD-OCT devices with higher resolution up to 3.8 μm. This must be taken into consideration designing future studies. Higher myopic refraction should be excluded or properly matched between groups. Furthermore, normative databases are needed to be refraction adjusted.

The main aim of the study was not to characterize RNFLT in MS population. Therefore, the MS population involved was randomly selected and examiner was not blinded to subjects' diagnosis and history of optic neuritis. Furthermore, the groups were not gender- or age-matched and both eyes of each subject were included. However, this was not a major issue in comparing RNFLT in the same

subject between two different machines and did not affect the results of our main study aim.

Conflict of Interests

None of the authors had any conflict of interests.

Acknowledgments

A. P. Lange was funded by the Swiss National Science Foundation and the UBC Hospital NMO Research Program.

References

[1] D. Huang, E. A. Swanson, C. P. Lin et al., "Optical coherence tomography," *Science*, vol. 254, no. 5035, pp. 1178–1181, 1991.

[2] L. A. Paunescu, J. S. Schuman, L. L. Price et al., "Reproducibility of nerve fiber thickness, macular thickness, and optic nerve head measurements using StratusOCT," *Investigative Ophthalmology and Visual Science*, vol. 45, no. 6, pp. 1716–1724, 2004.

[3] C. K. S. Leung, C. Ye, R. N. Weinreb et al., "Retinal nerve fiber layer imaging with spectral-domain optical coherence tomography. A study on diagnostic agreement with Heidelberg retinal tomograph," *Ophthalmology*, vol. 117, no. 2, pp. 267–274, 2010.

[4] A. Sakamoto, M. Hangai, and N. Yoshimura, "Spectral-domain optical coherence tomography with multiple B-scan averaging for enhanced imaging of retinal diseases," *Ophthalmology*, vol. 115, no. 6, pp. 1071–1078, 2008.

[5] R. T. Chang, O. J. Knight, W. J. Feuer, and D. L. Budenz, "Sensitivity and specificity of time-domain versus spectral-domain optical coherence tomography in diagnosing early to moderate glaucoma," *Ophthalmology*, vol. 116, no. 12, pp. 2294–2299, 2009.

[6] O. J. Knight, R. T. Chang, W. J. Feuer, and D. L. Budenz, "Comparison of retinal nerve fiber layer measurements using time domain and spectral domain optical coherent tomography," *Ophthalmology*, vol. 116, no. 7, pp. 1271–1277, 2009.

[7] C. K. S. Leung, C. Y. L. Cheung, R. N. Weinreb et al., "Retinal nerve fiber layer imaging with spectral-domain optical coherence tomography: a variability and diagnostic performance study," *Ophthalmology*, vol. 116, no. 7, pp. 1257–1263, 2009.

[8] K. R. Sung, D. Y. Kim, S. B. Park, and M. S. Kook, "Comparison of retinal nerve fiber layer thickness measured by Cirrus HD and Stratus optical coherence tomography," *Ophthalmology*, vol. 116, no. 7, pp. 1264–1270, 2009.

[9] G. Vizzeri, R. N. Weinreb, A. O. Gonzalez-Garcia et al., "Agreement between spectral-domain and time-domain OCT for measuring RNFL thickness," *British Journal of Ophthalmology*, vol. 93, no. 6, pp. 775–781, 2009.

[10] J. S. Kim, H. Ishikawa, K. R. Sung et al., "Retinal nerve fibre layer thickness measurement reproducibility improved with spectral domain optical coherence tomography," *British Journal of Ophthalmology*, vol. 93, no. 8, pp. 1057–1063, 2009.

[11] A. O. Gonzalez-Garcia, G. Vizzeri, C. Bowd, F. A. Medeiros, L. M. Zangwill, and R. N. Weinreb, "Reproducibility of RTVue retinal nerve fiber layer thickness and optic disc measurements and agreement with Stratus optical coherence tomography measurements," *American Journal of Ophthalmology*, vol. 147, no. 6, pp. 1067–1074, 2009.

[12] L. K. Seibold, N. Mandava, and M. Y. Kahook, "Comparison of retinal nerve fiber layer thickness in normal eyes using time-domain and spectral-domain optical coherence tomography," *American Journal of Ophthalmology*, vol. 150, no. 6, pp. 807–814, 2010.

[13] S. N. Arthur, S. D. Smith, M. M. Wright et al., "Reproducibility and agreement in evaluating retinal nerve fibre layer thickness between Stratus and Spectralis OCT," *Eye*, vol. 25, no. 2, pp. 192–200, 2011.

[14] G. M. Watson, J. L. Keltner, E. K. Chin, D. Harvey, A. Nguyen, and S. S. Park, "Comparison of retinal nerve fiber layer and central macular thickness measurements among five different optical coherence tomography instruments in patients with multiple sclerosis and optic neuritis," *Journal of Neuro-Ophthalmology*, vol. 31, no. 2, pp. 110–116, 2011.

[15] M. Bock, A. U. Brandt, J. Dörr et al., "Time domain and spectral domain optical coherence tomography in multiple sclerosis: a comparative cross-sectional study," *Multiple Sclerosis*, vol. 16, no. 7, pp. 893–896, 2010.

[16] C. H. Polman, S. C. Reingold, G. Edan et al., "Diagnostic criteria for multiple sclerosis: 2005 Revisions to the "McDonald Criteria"," *Annals of Neurology*, vol. 58, no. 6, pp. 840–846, 2005.

[17] U. E. K. Wolf-Schnurrbusch, L. Ceklic, C. K. Brinkmann et al., "Macular thickness measurements in healthy eyes using six different optical coherence tomography instruments," *Investigative Ophthalmology and Visual Science*, vol. 50, no. 7, pp. 3432–3437, 2009.

[18] A. Giani, M. Cigada, N. Choudhry et al., "Reproducibility of retinal thickness measurements on normal and pathologic eyes by different optical coherence tomography instruments," *American Journal of Ophthalmology*, vol. 150, no. 6, pp. 815–824, 2010.

[19] M. Pulicken, E. Gordon-Lipkin, L. J. Balcer, E. Frohman, G. Cutter, and P. A. Calabresi, "Optical coherence tomography and disease subtype in multiple sclerosis," *Neurology*, vol. 69, no. 22, pp. 2085–2092, 2007.

[20] M. S. Zaveri, A. Conger, A. Salter et al., "Retinal imaging by laser polarimetry and optical coherence tomography evidence of axonal degeneration in multiple sclerosis," *Archives of Neurology*, vol. 65, no. 7, pp. 924–928, 2008.

[21] L. S. Talman, E. R. Bisker, D. J. Sackel et al., "Longitudinal study of vision and retinal nerve fiber layer thickness in multiple sclerosis," *Annals of Neurology*, vol. 67, no. 6, pp. 749–760, 2010.

[22] J. N. Ratchford, M. E. Quigg, A. Conger et al., "Optical coherence tomography helps differentiate neuromyelitis optica and MS optic neuropathies," *Neurology*, vol. 73, no. 4, pp. 302–308, 2009.

[23] S. A. Trip, P. G. Schlottmann, S. J. Jones et al., "Retinal nerve fiber layer axonal loss and visual dysfunction in optic neuritis," *Annals of Neurology*, vol. 58, no. 3, pp. 383–391, 2005.

[24] J. B. Fisher, D. A. Jacobs, C. E. Markowitz et al., "Relation of visual function to retinal nerve fiber layer thickness in multiple sclerosis," *Ophthalmology*, vol. 113, no. 2, pp. 324–332, 2006.

[25] F. Costello, S. Coupland, W. Hodge et al., "Quantifying axonal loss after optic neuritis with optical coherence tomography," *Annals of Neurology*, vol. 59, no. 6, pp. 963–969, 2006.

[26] F. Costello, W. Hodge, Y. I. Pan, E. Eggenberger, S. Coupland, and R. H. Kardon, "Tracking retinal nerve fiber layer loss after optic neuritis: a prospective study using optical coherence tomography," *Multiple Sclerosis*, vol. 14, no. 7, pp. 893–905, 2008.

[27] F. Costello, W. Hodge, Y. I. Pan, M. Freedman, and C. DeMeulemeester, "Differences in retinal nerve fiber layer atrophy between multiple sclerosis subtypes," *Journal of the Neurological Sciences*, vol. 281, no. 1-2, pp. 74–79, 2009.

[28] A. P. D. Henderson, S. A. Trip, P. G. Schlottmann et al., "A preliminary longitudinal study of the retinal nerve fiber layer in progressive multiple sclerosis," *Journal of Neurology*, vol. 257, no. 7, pp. 1083–1091, 2010.

[29] A. P. D. Henderson, S. A. Trip, P. G. Schlottmann et al., "An investigation of the retinal nerve fibre layer in progressive multiple sclerosis using optical coherence tomography," *Brain*, vol. 131, no. 1, pp. 277–287, 2008.

[30] F. M. Rauscher, N. Sekhon, W. J. Feuer, and D. L. Budenz, "Myopia affects retinal nerve fiber layer measurements as determined by optical coherence tomography," *Journal of Glaucoma*, vol. 18, no. 7, pp. 501–505, 2009.

[31] M. Skaf, A. B. Bernardes, J. A. Cardillo et al., "Retinal nerve fibre layer thickness profile in normal eyes using third-generation optical coherence tomography," *Eye*, vol. 20, no. 4, pp. 431–439, 2006.